Monthly Notices
of the
ROYAL ASTRONOMICAL SOCIETY

MNRAS **484,** 1506–1525 (2019)
Advance Access publication 2019 January 07

doi:10.1093/mnras/stz036

Supernovae kicks in hierarchical triple systems

Cicero X. Lu [1,2]★ and Smadar Naoz [1,3]

[1]*Department of Physics and Astronomy, University of California, Los Angeles, CA 90095, USA*
[2]*Department of Physics and Astronomy, Johns Hopkins University, MD 21218, USA*
[3]*Mani L. Bhaumik Institute for Theoretical Physics, Department of Physics and Astronomy, UCLA, Los Angeles, CA 90095, USA*

Accepted 2018 December 31. Received 2018 December 31; in original form 2018 May 30

ABSTRACT

Most massive stars, if not all, are in binary configuration or higher multiples. These massive stars undergo supernova explosions and end their lives as either black holes or neutron stars. Recent observations have suggested that neutron stars and perhaps even black holes receive large velocity kicks at birth. Such natal kicks and the sudden mass-loss can significantly alter the orbital configuration of the system. Here we derive general analytical expressions that describe the effects of natal kicks in binaries on hierarchical triple systems. We explore several proof-of-concept applications such as black hole and neutron stars binaries and X-ray binaries with either stellar or Supermassive Black Hole (SMBH) companions on a wide orbit. Kicks can disrupt the hierarchical configuration, although it is harder to escape the potential well of an SMBH. Some binary systems do escape the SMBH system resulting in hypervelocity binary system. Furthermore, kicks can result in increasing or decreasing the orbital separations. Decreasing the orbital separation may have significant consequences in these astrophysical systems. For example, shrinking the separation post-supernova kick can lead to the shrinking of an inner compact binary that then may merge via gravitational wave (GW) emission. This process yields a supernova that is shortly followed by a possible GW–LIGO event. Interestingly, we find that the natal kick can result in shrinking the outer orbit, and the binary may cross the tertiary Roche limit, breaking up the inner binary. Thus, in the case of SMBH companion, this process can lead to either a tidal disruption event or a GW–LISA detection event (Extreme Mass ratio inspiral, EMRI) with a supernova precursor.

Key words: stars: evolution – stars: kinematics and dynamics – X-rays: binaries – gravitational waves.

1 INTRODUCTION

The majority of massive stars reside in a binary system ($\gtrsim$70 per cent for OBA spectral type stars; see Raghavan et al. 2010). In addition, observational campaigns have suggested that probably many of these stellar binaries are in fact triples or higher multiple configurations (e.g. Tokovinin 1997; Pribulla & Rucinski 2006; Eggleton, Kisseleva-Eggleton & Dearborn 2007; Tokovinin 2008; Borkovits et al. 2016). From dynamical stability arguments these must be hierarchical triples, in which the (inner) stellar binary is orbited by a third star on a much longer orbital period. Therefore, in most cases the dynamical behaviour of these systems takes place on time-scales much longer than the orbital periods. Recent developments in the study of the dynamics of hierarchical triples showed that these systems have rich and exciting behaviours. Specifically, it was shown that the inner orbital eccentricity can reach very high values and the mutual inclination between the two orbits can flip from below 90° to above 90°, namely the Eccentric Kozai–Lidov (EKL) mechanism (see for review Naoz 2016).

Stellar evolution plays an important role in the orbital dynamical evolution of massive stellar systems (e.g. Sana et al. 2012). For example, as the star evolves beyond the main sequence, it losses mass and expand it radius, which can have significant effects on the dynamics of these triple systems (e.g. Perets & Kratter 2012; Shappee & Thompson 2013; Michaely & Perets 2014; Naoz et al. 2016; Stephan et al. 2016; Toonen, Hamers & Portegies Zwart 2016; Stephan, Naoz & Zuckerman 2017). Most notability massive stars ($>8\,M_{\odot}$) undergo a Supernova (SN) explosion of which the star losses a significant fraction of its mass over short amount of time. Including SN kick to these systems can trigger eccentricity excitations and inclination flips in systems that pre-SN where unfavourable to the EKL mechanism. Of course SN kicks can also unbind the system (e.g. Michaely, Ginzburg & Perets 2016; Parker 2017)

★ E-mail: cicerolu@jhu.edu

Observations of pulsar proper motions in the last decade have shown that neutron stars (NSs) receive a large 'natal' kick velocity (with an average birth velocity of 200–500 km s^{-1}) as a result of SN asymmetry (e.g. Hansen & Phinney 1997; Lorimer, Bailes & Harrison 1997; Cordes & Chernoff 1998; Fryer, Woosley & Hartmann 1999; Hobbs et al. 2004, 2005; Beniamini & Piran 2016). Furthermore, it was shown that spin–orbit misalignment in pulsar binary systems requires a natal kick (Lai, Bildsten & Kaspi 1995; Kalogera 1996; Kaspi et al. 1996; Kalogera, Kolb & King 1998; Kalogera 2000). The survival of compact object binary systems is extremely interesting in light of the recent Laser Interferometer Gravitational-wave Observatory (LIGO) detection of Black Hole (BH) and NS binary mergers through gravitational waves (GWs) emission (e.g. Abbott et al. 2016c; LIGO Scientific and Virgo Collaboration 2017; Abbott et al. 2016b, 2017a). Either of these configurations' progenitors have undergone SN explosion and perhaps even a kick.

An analytical description of the effect of an SN kick on a binary system was studied in great details for circular binaries (Hills 1983; Kalogera 1996; Tauris & Takens 1998; Kalogera 2000; Hurley, Tout & Pols 2002), mainly for neutron stellar systems. Later, Belczynski et al. (2006) conducted a numerical analysis of BH eccentric binaries. Later Michaely et al. (2016) conducted a population synthesis models in binary systems exploring a larger range of parameter space. Furthermore, recent studies have shown that SNs in binaries at the Galactic centre can generate hypervelocity stars (Zubovas, Wynn & Gualandris 2013). Recently, Hamers (2018) derived a Hamiltonian formalism description to include external perturbations in hierarchical triple systems. These seminal studies showed that SN kicks play a crucial role in the formation of the spin–orbit misalignment in NS binaries that will affect their gravitational radiation waveforms. Here we expand upon these works and study the effect of SN kicks on triple systems considering a wide range of masses.

Here we explore SN kicks in the inner binary of a hierarchical stellar system with an arbitrary inclination and eccentricity.[1] We focus on both triple stellar systems as well as binary stars near an SMBH. It was recently suggested that binaries are prevalent in the Galactic centre. Observationally, there are currently three confirmed binaries in the Galactic centre (e.g. Ott, Eckart & Genzel 1999; Martins et al. 2006; Pfuhl et al. 2014). Moreover, it was estimated that the total massive binary fraction in the Galactic centre is comparable to the Galactic binary fraction (e.g. Ott et al. 1999; Rafelski et al. 2007). Furthermore, the recent observations of a gas-like object that plunges towards the Super Massive BH (SMBH) in the centre of the Galaxy (e.g. Gillessen et al. 2012), known as G2, provided another piece of evidence for the high likelihood of the existence of young binary systems (e.g. Witzel et al. 2014, 2017; Stephan et al. 2016; Bortolas, Mapelli & Spera 2017). Theoretically, Stephan et al. (2016) showed that the binary fraction in the nuclear star cluster might be as high as 70 per cent compared to the initial binary fraction, following a star formation episode that took place in that region a few Myr ago (e.g. Lu et al. 2013). In addition, it was recently suggested that the puzzling observations associated with the stellar disc in the centre of our Galaxy may provide indirect evidence of a large binary fraction (Naoz et al. 2018).

[1]Note that we neglect the interaction of the SN ejecta with the companion star since the effect of ejecta-companion interaction is small (e.g. Hirai, Podsiadlowski & Yamada 2018).

Our paper is organized as follows: we first describe the set-up of our systems (Section 2). We then derive the analytical expression for the relevant orbital parameters (Section 3) and consider a few different applications (Section 4). Specifically, consider applications to potential LIGO sources (Section 4.1), specifically, double NS systems (Section 4.1.3), NS–BH binaries (Section 4.1.1), and BH binaries sources (Section 4.1.2). We then we consider SN kicks in Low-mass X-ray binaries (Section 4.2) for an NS (Section 4.2.1) and BH (Section 4.2.2) compact object. We offer our discussion in Section 5.

2 SYSTEM SET-UP

Throughout this paper we consider the hierarchical triple system that consists of a tight binary (m_1 and m_2) and a third body (m_3) on a much wider orbit. The frame of reference chosen here is the invariable plane defined such that the z-axis is parallel to the total angular momentum of the system $\boldsymbol{G}_{\rm tot}$ (note that we are using the Delaunay's elements to denote the orbital parameters; see Valtonen & Karttunen 2006). Due to the hierarchical nature of the system the dominant motion of the triple can be reduced into two separate Keplerian orbits: the first describing the relative tight orbit of bodies m_1 and m_2, and the second describing the wide orbit of body m_3 around the centre of mass of bodies m_1 and m_2. In this frame we define the orbital parameters, i.e. the semimajor axes (SMAs) and the eccentricity of the inner and outer orbits as a_1, e_1, and a_2, e_2, respectively. The inclination of the inner (outer) orbit i_1 (i_2) is defined as the angle between the inner (outer) orbit's angular momentum $\boldsymbol{G}_1$ ($\boldsymbol{G}_2$) and the total angular momentum $\boldsymbol{G}_{\rm tot}$. The mutual inclination is defined as $i_{\rm tot} = i_1 + i_2$.

Without loss of generality we allow m_2 to undergo SN instantaneously, i.e. on a time-scale shorter than the orbital period, associated with a kick velocity $\boldsymbol{v}_{\rm k} = (v_x, v_y, v_z)$. Given a magnitude $v_{\rm k}$ the direction of the kick velocity vector can be determined by the angles θ and α defined such that

$$\boldsymbol{v}_r \cdot \boldsymbol{v}_{\rm k} = v_{\rm k} v_r \cos\theta \tag{1}$$

$$\boldsymbol{r} \cdot \boldsymbol{v}_{\rm k} = v_{\rm k} r \cos\alpha, \tag{2}$$

where $\boldsymbol{r}$ and $\boldsymbol{v}_r$ are defined in Fig. 1, with respect to the plane of the inner orbit.[2] The magnitude of the position vector is simply

$$r = \frac{a_1(1-e_1^2)}{1+e_1\cos f_1} = a_1(1-e_1\cos E_1), \tag{3}$$

where f_1 is the true anomaly of the inner orbit at the time of the explosion. The eccentric anomaly E_1 is related to the true anomaly f_1 by

$$\tan\frac{f_1}{2} = \sqrt{\frac{1+e_1}{1-e_1}}\tan\frac{E_1}{2} \tag{4}$$

(e.g. Murray & Dermott 2000). We will use the eccentric anomaly for our expressions below. The magnitude of the velocity is

$$v_r = \sqrt{\mu\left(\frac{2}{r}-\frac{1}{a_1}\right)} = v_{\rm c}\sqrt{\frac{1+e_1\cos E_1}{1-e_1\cos E_1}}, \tag{5}$$

[2]Note that while the definition of θ is consistent with that of Kalogera (2000), we choose to define the second angle in a different way.

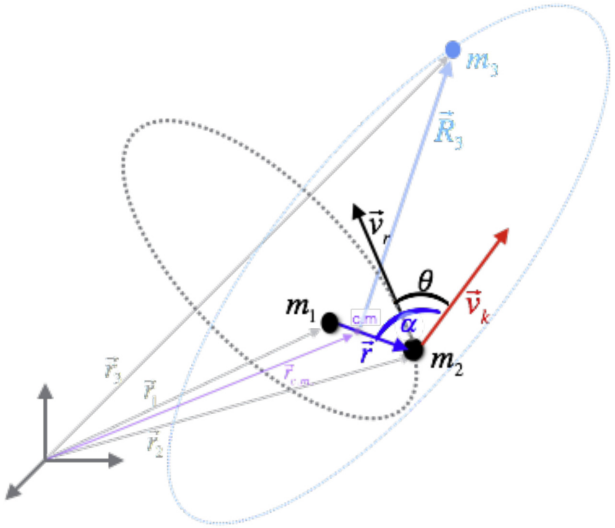

Figure 1. Schematic representation of the system (not to scale). Without the loss of generality we chose m_2 to undergo SN (see the text for details).

where $v_c = \sqrt{\mu/a_1}$ is the velocity of a circular orbit and $\mu = G(m_1 + m_2)$. The scalar product between the orbital velocity and the position vector has a simple relation, using the above definitions,

$$\begin{aligned}\boldsymbol{v}_r \cdot \boldsymbol{r} &= v_r r \cos\eta \\ &= v_c r \frac{e_1 \sin f_1}{\sqrt{1-e_1^2}} = v_c a_1 e_1 \sin E_1. \end{aligned} \tag{6}$$

From this we find that

$$\cos\eta = \frac{e_1 \sin E_1}{\sqrt{1 - e_1^2 \cos^2 E_1}}. \tag{7}$$

Using η the geometry in Fig. 1 yields boundary limits for α, i.e.

$$\theta - \eta \leq \alpha \leq \theta + \eta. \tag{8}$$

3 POST-SN ORBITAL PARAMETERS

We consider a system described in Fig. 1 with subscript '1' for the inner orbit and '2' for the outer orbit. We denote the post-SN orbital parameters with a subscript 'n'. The post-SN velocity vector of the new inner orbit is $\boldsymbol{v}_{r,n} = \boldsymbol{v}_r + \boldsymbol{v}_k$. The new velocity can be written as

$$v_{r,n}^2 = (\boldsymbol{v}_r + \boldsymbol{v}_k)^2 = G(m_1 + m_{2,n})\left(\frac{2}{r} - \frac{1}{a_{1,n}}\right) \tag{9}$$

and for instantaneous explosion we have $r = r_n$ (e.g. Kalogera 2000) and thus we can solve for the new SMA and find

$$\frac{a_{1,n}}{a_1} = \frac{\beta(1 - e_1 \cos E_1)}{2\beta - (1 + e_1 \cos E_1)(1 + u_k^2 + 2u_k \cos\theta)}, \tag{10}$$

where

$$\beta = \frac{m_1 + m_{2,n}}{m_1 + m_2}. \tag{11}$$

The normalized velocity is $\boldsymbol{u}_k = v_k/v_r$. Note that when $e_{1,0} \to 0$, equation (10) reduced to the relation founds in Kalogera (2000). Since the new SMA needs to be positive, it implies that a bound orbit will take place only if the denominator in equation (10) will be positive. In other words, a bound orbit will take place if

$$2\beta > (1 + e_1 \cos E_1)(1 + u_k^2 + 2u_k \cos\theta). \tag{12}$$

Solving for u_k we can find the maximum kick velocity that will allow a bound inner binary. This gives the range of u_k

$$u_{k,\min} \leq u_k \leq -\cos\theta + \sqrt{\frac{2\beta}{1 + e_1 \cos E_1} - \sin^2\theta}, \tag{13}$$

where

$$u_{k,\min} = \max\left(0, -\cos\theta \pm \sqrt{\frac{2\beta}{1 + e_1 \cos E_1} - \sin^2\theta}\right). \tag{14}$$

As can be seen from this equation, since $1 + e_1 \cos E_1$ can range between 0 and 2 and $\sin^2\theta \leq 1$, it implies that larger β allows for larger range of solutions. The maximum u_k and the post-SN SMA for a nominal choice of initial parameters is depicted in Fig. 2. It is interesting to note, as depicted in the figure, the maximum u_k increases with eccentricity when the SN takes place at apocentre. Furthermore, from equation (10), it is clear that if $\beta > 1 + u_k^2 + 2u_k \cos\theta$ then the post SMA *decreases* with respect to the pre-SN one. In other words,

$$\frac{a_{1,n}}{a_1} < 1 \quad \text{if} \quad \beta > 1 + u_k^2 + 2u_k \cos\theta \tag{15}$$

and

$$\frac{a_{1,n}}{a_1} > 1 \quad \text{if} \quad \beta < 1 + u_k^2 + 2u_k \cos\theta. \tag{16}$$

We note that the fraction is of course positive at all times.

An interesting limit can be reached when $u_k \to 0$, the sudden mass-loss shifts the centre of mass and a new SMA can be found by

$$a_{1,n}(u_k \to 0) = \frac{a_1 \beta(1 - e_1 \cos E_1)}{2\beta - 1 - e_1 \cos E_1}. \tag{17}$$

The new inner orbit eccentricity can be found from the expression for the angular momentum $h_{1,n} = \sqrt{G(m_1 + m_{2,n})a_{1,n}(1 - e_{1,n}^2)}$, where

$$\boldsymbol{h}_{1,n} = \boldsymbol{r} \times \boldsymbol{v}_{r,n}. \tag{18}$$

Thus, solving for $e_{1,n}$ we find that

$$e_{1,n}^2 = 1 - \frac{|\boldsymbol{r} \times (\boldsymbol{v}_r + \boldsymbol{v}_k)|^2}{a_{1,n} G(m_1 + m_{2,n})}. \tag{19}$$

Note that as both the numerator and denominator are proportional to a_1, it cancels out and thus $e_{1,n}$ does not depend on a_1. This yields another conditions for bound orbit for which $e_1 \cos E_1 > 1$. This has a simple dependence in the orbital parameters, and its a simple equation of e_1, u_k, α, θ, and E_1 (see equation A1) in Appendix A.

Using the eccentricity vector one can simply find the tilt angle between the pre- and post-SN orbital plane, which is associated with the spin–orbit misalignment angle (see Appendix B; e.g. equation B2).

Considering the outer orbit, we define the position vector $\boldsymbol{R}_3$ from the centre of mass of the inner orbit to the third object (see the schematic representation in Fig. 1). The magnitude of this vector is

$$R_3 = a_2(1 - e_2 \cos E_2), \tag{20}$$

where E_2 is the eccentric anomaly of the outer orbit at the time the SN in the inner orbit took place. The magnitude of the outer orbit velocity is

$$V_3 = \sqrt{\mu_3\left(\frac{2}{R_3} - \frac{1}{a_2}\right)} = V_{c3}\sqrt{\frac{1 + e_2 \cos E_2}{1 - e_2 \cos E_2}}, \tag{21}$$

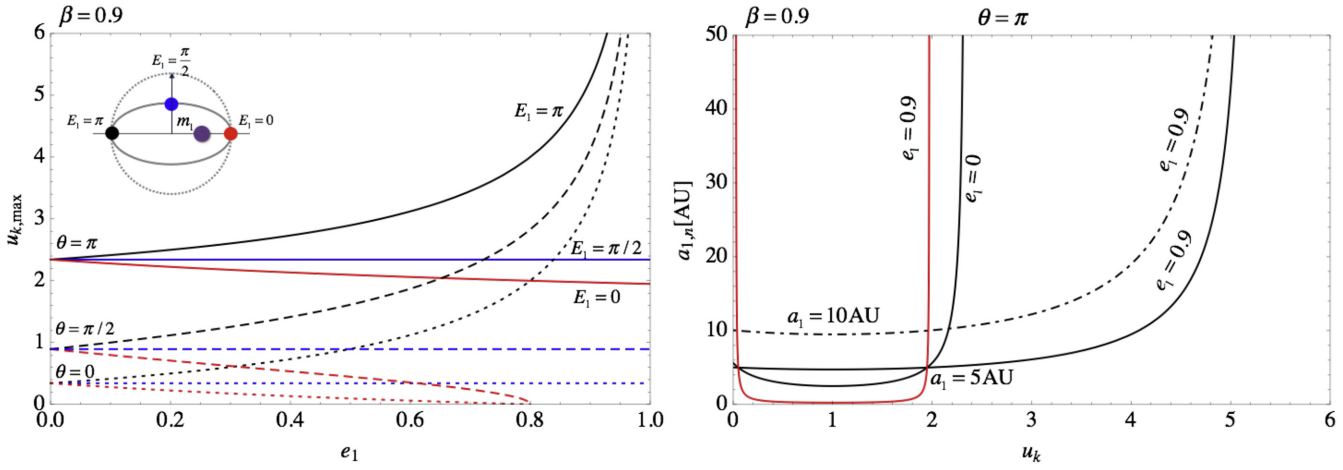

Figure 2. Inner binary orbital parameters, *left-hand panel:* The maximum dimensionless kick velocity $u_{\rm k,max} = \max(v_{\rm k}/v_r)$ as a function of the initial inner eccentricity e_1 (see equation 13). We consider three values for the eccentric anomaly $E_1 = 0$, $\pi/2$, and π, red, blue, and black lines, respectively (see top left schematic representation for the orbital configuration). We also consider three possible θ values (the angle between the kick velocity vector and $\mathbf{v}_r$), as labelled. *Right-hand panel:* The post-SN SMA, $a_{1,n}$ as a function of $u_{\rm k}$ (see equation 10). We consider initial SMA $a_1 = 5$ AU and show one example for $a_1 = 10$ AU (dot-dashed line). The colour code follows the left-hand panel, i.e. black lines are for $E_1 = \pi$ and red line for $E_1 = 0$. The initial eccentricity is labelled.

where $V_{c3} = \sqrt{\mu_3/a_2}$ is the velocity of a circular orbit and $\mu_3 = G(m_1 + m_2 + m_3)$. Similar to equation (9) we can write the post-SN outer orbit velocity as

$$V_{3,n}^2 = G(m_1 + m_{2,n} + m_3)\left(\frac{2}{R_3} - \frac{1}{a_{2,n}}\right) = \left(\boldsymbol{V}_3 - \frac{m_1(m_{2,n} - m_2)\boldsymbol{v}_r}{(m_1 + m_{2,n})(m_1 + m_2)} + \frac{m_{2,n}}{m_1 + m_{2,n}}\boldsymbol{v}_k\right)^2. \quad (22)$$

For the derivation that led to the last transition see Appendix C. This equation can now be used to find $a_{2,n}$. Simplifying it, we can write

$$\frac{1}{a_{2,n}} = \frac{2}{a_2(1 - e_2\cos E_2)} - \frac{f_v^2}{G(m_1 + m_{2,n} + m_3)}, \quad (23)$$

where f_v^2 is the right-hand side of equation (22) and f_v^2 is the right-hand side of equation (22), i.e.,

$$f_v^2 = \left(\boldsymbol{V}_3 - \frac{m_1(m_{2,n} - m_2)\boldsymbol{v}_r}{(m_1 + m_{2,n})(m_1 + m_2)} + \frac{m_{2,n}}{m_1 + m_{2,n}}\boldsymbol{v}_k\right)^2. \quad (24)$$

Thus, the constraint that $a_{2,n} \geq 0$ can be easily satisfied for a large m_3. Interestingly, when m_3 is large such that the second term in equation (23) goes to zero, the post-SN kick outer orbits SMA, $a_{2,n}$, may shrink.

Similar to equation (19), we can find the post-SN outer orbit eccentricity

$$e_{2,n}^2 = 1 - \frac{1}{a_{2,n}G(m_1 + m_{2,n} + m_3)} \times \left|\boldsymbol{R}_3 \times \left(\boldsymbol{V}_3 - \frac{m_1(m_{2,n} - m_2)\boldsymbol{v}_r}{(m_1 + m_{2,n})(m_1 + m_2)} + \frac{m_{2,n}}{m_1 + m_{2,n}}\boldsymbol{v}_k\right)\right|^2. \quad (25)$$

The total angular momentum is simply

$$\boldsymbol{G}_{{\rm tot},n} = \boldsymbol{G}_{1,n} + \boldsymbol{G}_{2,n}, \quad (26)$$

where

$$\boldsymbol{G}_{1,n} = \frac{m_1 m_{2,n}}{m_1 + m_{2,n}}\boldsymbol{h}_{1,n} \quad (27)$$

and $\boldsymbol{h}_{1,n}$ is defined in equation (18) and similarly we can define $\boldsymbol{h}_{2,n} = \boldsymbol{R}_3 \times \boldsymbol{V}_{3,n}$ and $\boldsymbol{G}_{2,n}$. From these we can find the new mutual inclination (after transferring to the invariable plane):

$$\cos i_n = \frac{G_{{\rm tot},n}^2 - G_{1,n}^2 - G_{2,n}^2}{2G_{1,n}G_{2,n}}. \quad (28)$$

From the angular momentum vectors we can also deduce the line of nodes, and from there, using the eccentricity vectors of the inner and outer orbits one can infer the argument of periapsis of the inner and outer orbit SMA.

Note that similar equations have been derived in previous literature (e.g. Pijloo, Caputo & Portegies Zwart 2012; Toonen et al. 2016; Hamers 2018). We present derived equations here so that our notations can be self-contained.

4 APPLICATIONS

We present several representative numerical experiments aimed to explore a variety of astrophysical applications. These are meant to give a proof-of-concept for the types of possible outcomes. We note that the final result depends on the choice of initial conditions and that a full population synthesis or detailed Monte Carlo are beyond the initial scope of this paper. The numerical parameters are summarized in Table 1. In all of our numerical analyses below we work in the invariable plane. In all of our Pre-SN systems, we require a hierarchical system that satisfied the stability condition:

$$\epsilon = \frac{a_1}{a_2}\frac{e_2}{1 - e_2^2} \leq 0.1 \quad (29)$$

(e.g. Lithwick & Naoz 2011).

All of our pre-SN systems are beyond tidal disruption limit, i.e. $a_2(1 - e_2) > a_1(1 + e_1)(m_3/(m_1 + m_2))^{(1/3)}$. Furthermore, note that Naoz et al. (2013) showed that the ε criterion has a similar functional form as the Mardling & Aarseth (2001). We also checked that the Mardling & Aarseth (2001) criterion is satisfied for all of our similar mass systems (for which this criterion was devised). Stability of mass hierarchy was studied in the literature in great details (e.g. Ivanov, Polnarev & Saha 2005; Katz & Dong 2012; Hamers et al. 2013; Antognini et al. 2014; Antonini, Murray &

Table 1. Table of the numerical experiments run below. We show the masses of the inner binary (pre- and post-SN), the mass of the tertiary, and their SMA. We also present the fraction of systems out of all the runs that remained bound after the SN (column 9), and the fraction of triple systems that remained bound out of all the surviving binaries (column 10). We also show the fraction of systems at which one of the binary members crossed the inner Roche radius ($R_{\rm Roche,\,in}$, see equation 34) out of all binaries. The last column shows the fraction of systems of which one of the binary members crossed their tertiary Roche radius ($R_{\rm Roche,\,out}$; see equation 31) out of all *surviving triple* systems. For NS–NS and BH–BH cases we considered two SN explosions. MC represents Monte Carlo runs (see the text and Table 2 for more details). The details are specified in the text and for completeness we reiterate our Monte Carlo initial conditions here. $\rm MC^1$ refers to the Monte Carlo choices for a_1, which is chosen to be uniform in log space between $5\,\rm R_\odot$ and $1000\,\rm R_\odot$. $\rm MC^{2,EC}$, refers to the choice of a_2, from a uniform in log distribution with a minimum a_2 that is consistent with $\varepsilon = 0.1$ and maximum of 10 000 AU. The density of binary systems in this case is consistent with a_2^{-3} and thus we label it 'EC' for extreme cusp. $\rm MC^{2,BW}$ refers to the Monte Carlo choices of a_2 to be uniform, which is consistent with density of a_2^{-2} with a minimal value 100 AU and a maximum value of 0.1 pc (which is representative of a distribution around an SMBH; e.g. Bahcall & Wolf 1976). Note that the inner and outer SMA also satisfy $\varepsilon = 0.1$ criteria. In all of our Monte Carlo runs, the inner and outer eccentricities were chosen from uniform distribution and the mutual inclination was chosen from an isotropic distribution. The inner and outer arguments of pericentre and the mean anomaly were chosen from uniform distributions. Note that survival rate for binaries and triples refer to the systems that are bound instantaneously post-SNe. The inner binaries that crossed the Roche limit of each other and the binary systems that crossed the Roche limit of the tertiary body are included in the count of survived systems since the systems that are undergoing mass transfer still stay bound post-SNe instantaneously. We provide their percentages in separate columns for clarity.

Name	Sim	m_1 $\rm M_\odot$	$m_{1,\,n}$ $\rm M_\odot$	m_2 $\rm M_\odot$	$m_{2,\,n}$ $\rm M_\odot$	m_3 $\rm M_\odot$	a_1 $\rm R_\odot$	a_2 AU	Per cent Bin out of total	Per cent Triples out of Bin	Per cent in $R_{\rm Roche,\,in}$ out of Bin	Per cent in $R_{\rm Roche,\,out}$ out of 3	Per centescaped Bin
NS-LMXB	(a)	4	1.4	1	1	3	$\rm MC^1$	$\rm MC^{2,\,EC}$	4	0	0	0	100
	(b)	4	1.4	1	1	4×10^6	$\rm MC^1$	$\rm MC^{2,\,EC}$	4	94	0	4	6
	(c)	4	1.4	1	1	4×10^6	$\rm MC^1$	$\rm MC^{2,\,BW}$	4	99	0	2	1
BH-LMXB	(d)	9	7	1	1	3	$\rm MC^1$	$\rm MC^{2,\,EC}$	11	1	24	13	99
	(e)	9	7	1	1	4×10^6	$\rm MC^1$	$\rm MC^{2,\,EC}$	11	99	24	7	1
	(f)	9	7	1	1	4×10^6	$\rm MC^1$	$\rm MC^{2,\,BW}$	10	92	25	2	8
NS–BH	(g)	4	1.4	10	10	3	5	1000	33	0	0	0	100
	(h)	4	1.4	10	10	3	5	$\rm MC^{2,\,EC}$	33	0	0	0	100
	(i)	4	1.4	10	10	4×10^6	5	$\rm MC^{2,\,BW}$	33	99	0	0	1
	(j)	4	1.4	10	10	4×10^6	$\rm MC^1$	$\rm MC^{2,\,EC}$	12	71	0	2	29
	(k)	4	1.4	10	10	4×10^6	5	1000	33	100	0	1	0
									1st | 2nd	1st | 2nd	1st | 2nd	1st | 2nd	1st | 2nd	1st | 2nd
NS–NS	(l)	5	1.4	4	1.4	3	5	1000	20 | 0	0 | 0	0 | 0	0 | 0	0 | 7
(2 × SN)	(m)	5	1.4	4	1.4	3	5	$\rm MC^{2,\,EC}$	20 | 0	0 | 0	0 | 0	0 | 0	100 | 0
	(n)	5	1.4	4	1.4	4×10^6	5	$\rm MC^{2,\,BW}$	20 | 11	98 | 43	0 | 0	0 | 0	2 | 57
	(o)	5	1.4	4	1.4	4×10^6	5	1000	20 | 10	100 | 93	0 | 0	3 | 0	0 | 7
BH–BH	(p)	31	30	15	14	3	5	1000	47 | 0	0 | 0	0 | 0	0 | 0	100 | 100
(2 × SN)	(q)	31	30	15	14	3	5	$\rm MC^{2,\,EC}$	47 | 0	1 | 0	0 | 0	0 | 0	99 | 100
	(r)	31	30	15	14	4×10^6	5	$\rm MC^{2,\,BW}$	47 | 29	87 | 83	0 | 0	0 | 0	13 | 17
	(s)	31	30	15	14	4×10^6	5	1000	47 | 32	99 | 98	0 | 0	1 | 0	1 | 2

Mikkola 2014; Bode & Wegg 2014; Petrovich 2015), and indeed we have verified that not only the binaries around the SMBH are above the tidal disruption zone, and $\varepsilon > 0.1$ but also that they obey the stability criterion (e.g. Petrovich 2015) . We note that these stability criteria deem a system unstable if at any point in time it will encounter instability and does not take time-scale into consideration (e.g. Mylläri et al. 2018). Thus, we stress that using these criteria underestimate the number of allowable systems within their lifetime.

We note that we do not provide a population synthesis here; however, we estimate the quadruple-order time-scales of our systems to estimate how likely it is that they have underwent an EKL evolution before the SN kick took place. The systems will not be affected by secular effects before they undergo SN. We stress that this is a heuristic calculation because a self-consistent one would need to include both the post-main sequence stellar evolution effect on EKL which is beyond the scope of this paper (see for the dramatic implications of the interplay between EKL and post-main sequence evolution; e.g. Naoz 2016; Toonen et al. 2016; Stephan et al. 2016, 2017; Stephan, Naoz & Gaudi 2018).

We focus our discussion on the survival of the inner binary and the overall triple configurations as well as the possible outcomes. A kick can unbind the binary or the triple, or, to be more precise, if the post-SN orbital velocity is larger than the escape velocity of the system, the system becomes unbound. Note that the fraction of binaries surviving the SN kick is of course independent on the choice of tertiary companion. Although in the Solar neighbourhood, the most massive star is the tertiary in about 18 per cent of triples (Tokovinin, Hartung & Hayward 2010), we only focus on the scenario in which the inner binary undergoes SN first and when tertiary goes SN; it will not affect the parameters of inner orbit. Tertiary companion's SN affect on inner orbit is beyond the scope of this paper.

In all of our runs, we assume a normal distribution of kick velocities with an average of $400\,\rm km\,s^{-1}$ and a standard deviation of $265\,\rm km\,s^{-1}$ (e.g. Hansen & Phinney 1997; Arzoumanian, Chernoff & Cordes 2002; Hobbs et al. 2004). The tilt angle θ is chosen from a uniform distribution between 0 and 2π and α is then chosen from a uniform distribution for which the minimum and maximum values are set by equation (8). Furthermore, in all of our runs, the inclination angle was chosen to be isotropic (uniform in

Table 2. A summary of the Monte Carlo parameters. For the inner orbit's SMA, a_1, Monte Carlo simulations were chosen to be uniform, with the limits specified in the table. For the outer orbit, we have followed Hoang et al. (2018) Monte Carlo choice of stellar distribution around an SMBH. Specifically, we have chosen a Bahcall-Wolf (BW; e.g. Bahcall & Wolf 1977) distribution as well as an extreme cusp distribution. Note for N number of object we have $dN = 4\pi\, a_2^2\, n(a_2)\, da_2 = 4\pi\, a_2^3\, n(a_2)\, d(\ln a_2)$, and thus we choose to have the outer binary SMA follow a uniform distribution in a_2 for the BW distribution ($MC^{2,BW}$) and $\ln a_2$ Extreme cusp ($MC^{2,EC}$) distribution. We choose both the inner and outer orbit eccentricities, e_1 and e_2, respectively, from a uniform distribution between $0-1$, the argument of periapsis of the inner and outer orbits, ω_1 and ω_1, respectively, from a uniform distribution between $0^\circ - 180^\circ$, the mutual inclination was chosen from an isotropic distribution (uniform in cos$i$). See the text for more details.

Name	a_1	a_2
MC[1]	Uniform $5-1000\,R_\odot$	–
MC^{2,BW} Bahcall–Wolf	–	$n(a_2) \sim a_2^{-2}$ 100 AU–0.1 pc
MC^{2,EC} Extreme Cusp	–	$n(a_2) \sim a_2^{-3}$ $a_{2,\,min} \in \varepsilon = 0.1$ $a_{2,\,max} = 10^4$ AU

cos i) and the arguments of periapsis of the inner and outer orbits were chosen from a uniform distribution between 0 and 2π. The inner and outer eccentricities, e_1 and e_2, were chosen from a uniform distribution between $0-1$. The mean anomaly was chosen from a uniform distribution from which we solved for the true and eccentric anomalies (e.g. Savransky, Cady & Kasdin 2011; see Table 2 for details of the Monte Carlo simulations and how they depend on the SMA). We run a total of 10 000 systems for each tertiary mass.

4.1 GW sources

4.1.1 Neutron star–black hole binary–one natal kick

The formation scenario of NS–BH binary systems typically involves that after the first SN explosion, the compact remnant enters a common-envelope phase with its companion. This may lead to tightening of the orbit, and if the system remains bound after the companion star collapses, an NS–BH binary may form (e.g. Fryer et al. 1999; Dominik et al. 2012; Postnov & Yungelson 2014). These compact object binaries have been suggested to exist in the Galactic disc (e.g. Pfahl, Podsiadlowski & Rappaport 2005; Kiel & Hurley 2009), Galactic centre (e.g. Faucher-Giguère & Loeb 2011), and globular clusters (e.g. Sigurdsson et al. 2003). Recently, Abbott et al. (2016d) constrained the NS–BH binaries merger rate to be less than 3 600 $Gpc^{-3}\,yr^{-1}$ based on the non-detection so far.

As a proof-of-concept we run a Monte Carlo numerical experiment exploring the possible outcomes of triple systems. For these systems we assume that *only* the NS had a natal kick. We adopt Kalogera (2000) orbital parameters for the binary, with $m_1 = 10\,M_\odot$ and $m_2 = 4\,M_\odot$, and a post-SN mass of $1.4\,M_\odot$. We initially set $a_1 = 5\,R_\odot$. However, unlike Kalogera (2000), who adopted a circular initial (inner) orbit, we adopt a uniform eccentricity distribution between 0 and 1. We explore two systems with two different tertiaries, one with a stellar companion $m_3 = 3\,M_\odot$ and the other with $m_3 = 4 \times 10^6\,M_\odot$. In both examples we set $a_2 =$ 1000 AU and adopt a uniform distribution for e_2, while keeping the stability requirement specified in equation (29).

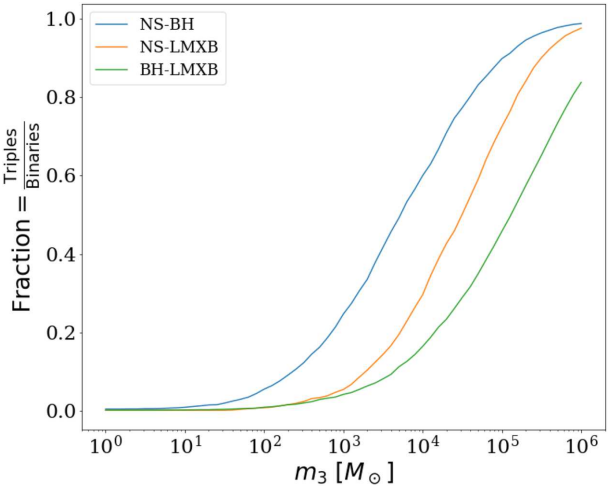

Figure 3. We show the fractions of triples over binaries that survived an NS–BH(NS–LMXB, BH–LMXB) one natal kick as a function of the tertiary mass. This is for systems of NS–BH with $a_1 = 5\,R_\odot$ and a_2 from $MC^{2,BW}$. For NS–LMXB and BH–LMXB, a_1 is chosen from MC^1 and a_2 from $MC^{2,EC}$.

In addition to these two runs, we also run a Monte Carlo run for the stellar companion by drawing a_2 from a distribution with a maximum of 1000 AU and a minimum a_2 that satisfy $\varepsilon = 0.1$. For the stellar-companion case we also run a Monte Carlo run for which a_2 is chosen from a lognormal distribution with a minimum that satisfied $\varepsilon = 0.1$ and a maximum of 10 000 AU. See Table 1 for a summary of the runs and outcomes and see Table 2 for the Monte Carlo parameters.

Furthermore, we also run the same set of Monte Carlo runs while setting $a_1 = 5$ AU to allow for a wider initial configuration (see Appendix E and Table E1 for the parameters). For these systems, we found that in this case a higher fraction of systems crossed the SMBH.

While the fraction of binaries surviving the SN kick is of course independent of the choice of tertiary, the survival of triples increase with the mass of the tertiary (as depicted in Fig. 3). As shown in this figure, the fraction of triple systems that remain bound after the SN occurred approaches the binary fraction for tertiaries with masses $\gtrsim 10^6\,M_\odot$. Note that this is a generic conclusion for all of our cases. Thus, in our SMBH companion case the fraction of systems that remain bound triples approaches the binary fraction (as depicted in the bottom panels of Fig. 4). This implies that mergers of compact binaries due to eccentricity-induced dynamical evolution such as EKL is more likely to take place in the presence of high-mass third companion (e.g. Hoang et al. 2018).

In Fig. 4, we show the dependence of the surviving systems on the kick velocity. In particular, we depict in the bottom panels, the distribution of the surviving binaries (triples), solid (dashed) lines, and in the top panels, we show the fraction of surviving systems out of the initial systems. We consider our two tertiary systems, stellar companion (left-hand column) and SMBH companion (right-hand column). As expected the fraction of systems that stay bound post-SN decreases as a function of the kick velocity induced (as seen in the top panel of Fig. 4). Specifically, in this figure we show the fraction of bound post-SN systems (f_{PostSN}) over the fraction of initial pre-SN systems ($f_{Pre\text{-}SN}$) at the same kick velocity bin. About 50 per cent of the binaries remained bound for kick velocities $\lesssim$300 km s^{-1}. Furthermore, about 0.3 per cent (50 per cent) of the

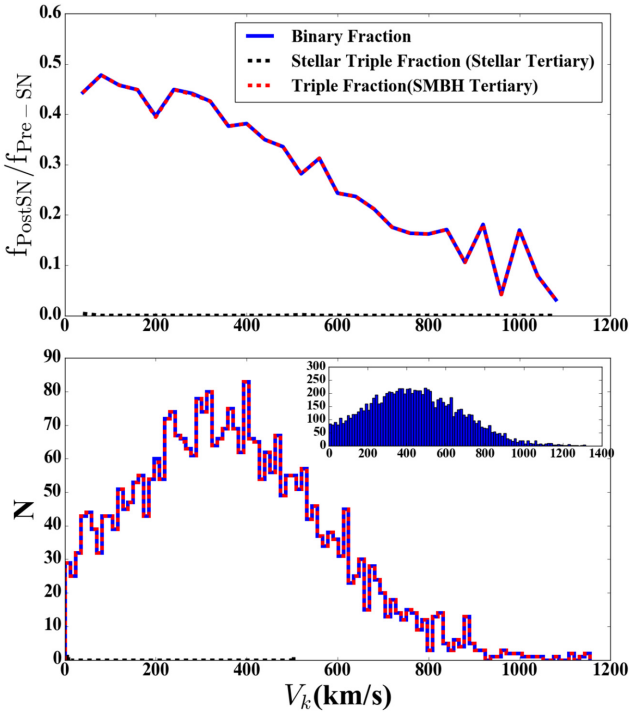

Figure 4. Kick velocity distribution of survived system in NS–BH binaries, one natal kick for $a_1 = 5\,R_\odot$ and $a_2 = 1000\,AU$, for stellar companion run (g) left and an SMBH companion run (k), right. In the *top panel* we consider the systems that remained bound post-SN with a distant stellar mass companion in black dotted line and with a distant SMBH companion with red dotted line. Note that the triple fraction is very low (nearly zero) with stellar companion. *Bottom panels:* show a histogram of the kick velocity of the survived binaries (solid lines) and triples (dashed lines). Note that the survived inner binaries are independent of the mass of the outer body. The inset in the bottom panel shows the initial distribution of the kick velocity v_k. Also note that in the case with SMBH as tertiary the two lines overlap.

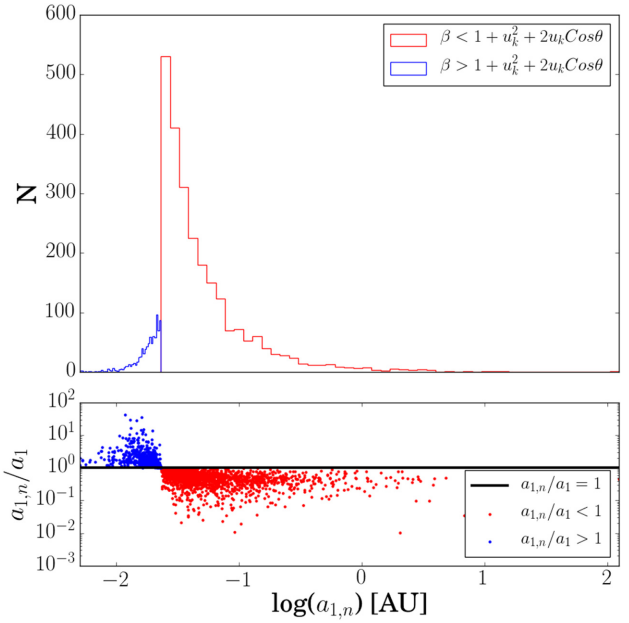

Figure 5. NS–BH inner binary SMA for system with $a_1 = 5\,R_\odot$ and a_2 from $MC^{2,BW}$, and an SMBH companion, run (i). We show a histogram (*top panel*) of the inner binary SMA after an SNe in the NS–BH system. We consider systems that their orbit expanded after the two SNs (red line), which corresponds to the last step $\beta < 1 + u_k^2 + 2u_k \cos\theta$, as well as systems that shrunk their orbits due to the SNs natal kicks (blue line, $\beta > 1 + u_k^2 + 2u_k \cos\theta$). In the *bottom panel* we show the semimajor axial ratio ($a_{1,n}/a_1$) as a function of the post-SN SMA.

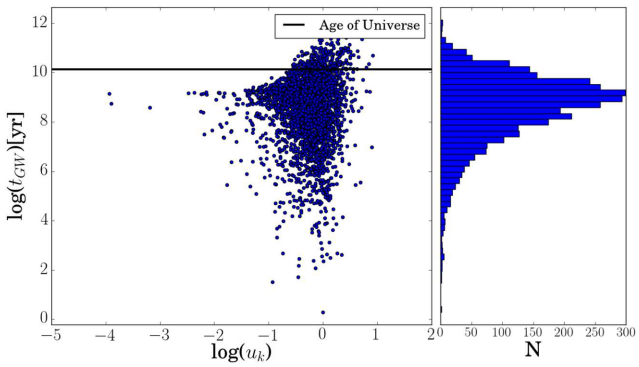

Figure 6. NS–BH GW time-scale for system with $a_1 = 5\,R_\odot$ and a_2 from $MC^{2,BW}$, and an SMBH companion, run (i). *Left-hand panel*: We show the GW time-scale as a function of the dimensionless kick velocity, u_k. In the *right-hand panel* we show the histogram of the GW time-scales.

triples remain bound for stellar mass (SMBH) tertiary and for the same kick velocity range. In the bottom panels, we show a histogram of the bound systems as a function of v_k.

Our analytical calculation showed that systems for which $\beta > 1 + u_k^2 + 2u_k \cos\theta$ will shrink their SMA after the natal kick. As depicted in Fig. 5, given the mass ratio, β, the tilt angle θ, and the dimensionless kick velocity u_k, we can predict if the orbit will shrink or expand.

Shrinking SMA following natal kick can have interesting consequences. For example, NS–BH binaries will merge by emitting GW emission (e.g. Peters & Mathews 1963; Peters 1964; Press & Thorne 1972) and here we use a scaling relation given by Blaes, Lee & Socrates (2002):

$$t_{gw} \approx 2.9\times10^{12}\mathrm{yr}\left(\frac{m_1}{10^6\,M_\odot}\right)^{-1}\left(\frac{m_{2,n}}{10^6\,M_\odot}\right)^{-1} \times\left(\frac{m_1+m_{2,n}}{2\times10^6_\odot}\right)^{-1}\left(\frac{a_1}{10^{-2}\,\mathrm{pc}}\right)^{-1}\times f(e_1)\left(1-e_1^2\right)^{7/2}. \quad (30)$$

We estimate the GW time-scale at which these binaries will merge for one of our proof-of-concept runs (see Fig. 6) and find an average merging time of $\sim10^{8.5}$ yr [for $a_1 = 5\,R_\odot$ and $a_2 = 1000\,AU$ system with an SMBH companion, i.e. run (i)]. We find somewhat shorter merger time-scale ($\sim10^6$ yr) of a Monte Carlo that considers an initial SMA binary of $a_1 = 5\,R_\odot$ and $a_2 = 1000\,AU$ system with stellar companion, i.e. run (g). As depicted in Fig. 6, the merger times are not overly sensitive to the dimensionless kick velocity u_k. This is consistent with our results and emphasize the sensitivity to initial conditions. Furthermore, we expect that near SMBH the merger time will shorten due to the EKL mechanism (e.g. Naoz 2016; Hoang et al. 2018).

We found that $\sim1-2$ per cent of all surviving triples in the Monte Carlo runs with SMBH tertiary crossed its Roche limit. In other words the resulting post-SN orbital parameters were

$$a_{2,n}(1-e_{2,n}) < a_{1,n}(1+e_{1,n})\left(\frac{m_3+m_{2,n}+m_1}{m_1+m_{2,n}}\right)^{1/3} \quad (31)$$

(e.g. Naoz & Silk 2014). This process will breakup the binary similar to the Hills process (e.g. Hills 1988; Yu & Tremaine 2003). In this case we have that one of the compact object will be on a close eccentric orbit around the SMBH, spiraling in via GW emission (i.e. Extreme Mass Ratio in spiral, EMRI). In particular, we note that for the wider initial binaries the SN kick results in Roche limit crossing between one member of the inner tight binary and the tertiary. For the most dramatic cases, the percentage of *mergers with the SMBH post-kick* is 1 per cent (for $a_1 = 5\,\mathrm{R}_\odot$) and ∼74 per cent (for $a_1 = 5$ au), see E1 case (k) and (k5). These events can result in EMRI via GW emission that may be a LISA source. In Fig. 7 we show the ratio of the left to the right-hand side of equation (31), up to the mass term, pre- and post-SN. We show the results for three of the proof-of-concept Monte Carlo runs we conducted around SMBH, (i), (j), and (k) (see Table 1). As depicted in all three cases, a non-negligible fraction of the systems crossed the SMBH Roche limit (shaded grey in the figure). Thus, resulting in having one member of the binary gaining high velocity and the other on a tight eccentric configuration that can spiral in via GW emission.

We found that a wider initial condition for a_1 dramatically decreases the percentage of survived binaries systems with stellar (SMBH) companion. We quantify the Roche limit crossing between the two inner members as $a_{1,n}(1 - e_{1,n}) \leq R_{\rm Roche}$, and

$$R_{\rm Roche} \sim 1.6 R_2 \left(\frac{m_{2,n}}{m_1 + m_{2,n}}\right)^{-1/3}, \tag{32}$$

where R_2 is the radius associated with $m_{2,n}$ that in this case is the radius of an NS. Given these new orbits, for the wider initial conditions, we calculate the GW emission time-scale for the systems that survived SNe kicks and the systems that survived the kicks but the inner binary crossed the Roche limit of the tertiary. We found a shorter merger rate compared to Fig. 6 (not shown to avoid clutter).

Our proof-of-concept simulations suggest that many of the survived systems will merge in less than the age of the Universe, with typical merger time-scale of a few Myr that can be as low as a few hundred years detectable by LISA (see Fig. 8). We consider the GW characteristic frequency (f) of the signal to be $f = v_{\rm p}/r_{\rm p}$, where $v_{\rm p}$ and $r_{\rm p}$ are the orbital velocity and the pericentre, and respectively,

$$f = 2\pi \frac{(1 + e_{\rm Hill})^{1/2}}{(1 - e_{\rm Hill})^{-3/2}} \frac{1}{P_{2,n}}, \tag{33}$$

where for simplicity we take the compact member (or the heavy member) of the inner binary to be the one who will merge with the SMBH (denote m), and set the new SMA to simply be $a_{2,n}$, and thus the $P_{2,n}$ is the post SN outer orbital period. The new eccentricity around the SMBH via the Hills process is estimated as: $e_{\rm Hill} \sim 1 - (m/m_3)^{1/3}$ (e.g. Hills 1988; Yu & Tremaine 2003). See Table 3 for a range of merger times after the SN. These results suggest that an SN remnant might serve as a signature for the process.

In Fig. 7, the ratio of $V_{3,n}/V_{\rm c,esc}$ is colour coded, where $V_{c,\rm esc} = \sqrt{2\mu_3/a_{2,n}}$ is the post-SN escape velocity from a circular orbit. As expected, further away from the SMBH the binary velocity is larger.[3] Note that systems that actually escape the SMBH potential well are not shown here, because they do not have a defined $a_{2,n}$. We do find that some fraction of the binary systems (depending on the initial conditions) will escape and unbind from the SMBH. Run (j) (of uniform Monte Carlo of the inner orbit's SMA and extreme cusp distribution around the SMBH) suggests that about 3 per cent out of all 29 per cent escaped binaries will be observed as hypervelocity binaries.

However, we note that those binaries with new velocities that are larger than $V_{\rm c,esc}$, may still be bound to the Galactic centre by the potential of the bulge, disc, or halo. To quantify this, we adopt a minimal velocity of $V_{3n} > 200\,\mathrm{km\,s^{-1}}$, following Portegies Zwart et al. (2006) who suggested that such a fast binary may escape the Galactic centre. For the NS–BH system discussed in this section, all of the systems that have $V_{3,n} > V_{\rm c,esc}$, also have $V_{3n} > 200\,\mathrm{km\,s^{-1}}$. However, this behaviour is highly sensitive to the initial conditions of the distribution of the binaries around the SMBH. In some later cases, we find that more than half of the system with velocity larger than the escape velocity will still remain bound to the Galactic centre. Note that in Tables 1 and E1, we consider escape from the SMBH, since this proof-of-concept calculation constraint to the three-body regime. We further found that for BH–NS binary with stellar companion, a third of all the escaped binary systems would have $V_{3n} > 200\,\mathrm{km\,s^{-1}}$.

4.1.2 *Black hole binaries–two natal kicks*

The recent detections of BH binaries (BHB; Abbott et al. 2016c,b; LIGO Scientific and Virgo Collaboration 2017) via LIGO revolutionized the field with the realization that the merger rate of BHB is now constrained to be between 9 and $240\,\mathrm{Gpc^{-3}\,yr^{-1}}$ (Abbott et al. 2016a). The astrophysical origin of these binaries is still under debate.

Many observational campaigns suggest that SN of BH progenitors have no natal kick associated with them (e.g. Willems et al. 2005; Reid et al. 2014; Ertl et al. 2016; Mandel 2016; Sukhbold et al. 2016). However, Repetto, Davies & Sigurdsson (2012) and Repetto & Nelemans (2015) suggested that BHs likely receive natal kicks similar in magnitude to NSs.[4] This is supported by the detection of one example of a non-negligible natal kick (e.g. Gualandris et al. 2005; Fragos et al. 2009). While it is still unclear what kick velocity magnitude if at all BH exhibit, it is clear that natal kick will affect the orbital configurations of these systems.

As a proof-of-concept we adopt the aforementioned natal kick distribution for each BH member. We adopt the following parameters for Monte Carlo simulations: The inner BH–BH progenitor orbit SMA was chosen to be $a_1 = 5\,\mathrm{R}_\odot$ while the outer orbit SMA was chosen to be $a_2 = 1000$ AU. We also performed a Monte Carlo simulation where a_2 was chosen from a uniform in log distribution (keeping $a_1 = 5\,\mathrm{R}_\odot$). The minimal value satisfied $\varepsilon = 0.1$ and a maximum value of 10 000 AU. We chose the initial mass of the BH progenitors to be $m_1 = 15\,\mathrm{M}_\odot$ and $m_2 = 31\,\mathrm{M}_\odot$, *just before the explosion*[5]. The heavier star after mass-loss went through mass-loss due to SN explosion and reduced its mass to $m_{2,n} = 30\,\mathrm{M}_\odot$. Shortly after the first SN event, the second star went through SN and resulted in $m_{1,n} = 14\,\mathrm{M}_\odot$ BH (e.g. Hurley, Pols & Tout 2000). As before, for the tertiary body, we used $3\,\mathrm{M}_\odot$ for stellar companion and $4 \times 10^6\,\mathrm{M}_\odot$ for SMBH companion. In the case of SMBH companion, we also run Monte Carlo simulations choosing a_2 from a Bahcall–Wolf-like distribution setting the density proportional to

[3] Note that an interesting observational detection of hypervelocity late-type-B stars is consistent with the velocity associated with SN kick in the Galactic Centre (e.g. Tauris & Takens 1998; Tauris & van den Heuvel 2014; Tauris 2015).

[4] Although Mandel (2016) suggested that these studies overestimate the inferred natal BH kick distribution.

[5] This means, of course, that the main-sequence mass were much larger.

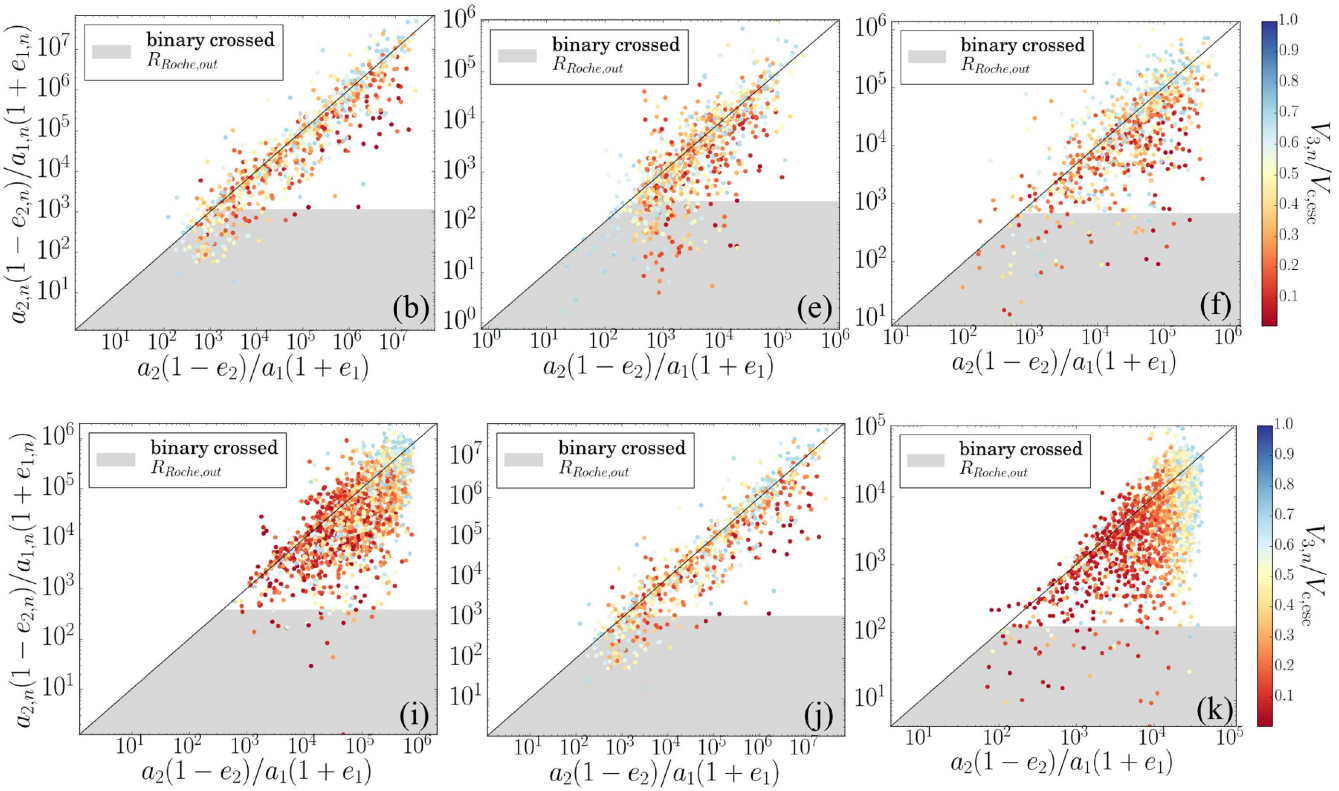

Figure 7. SMBH Roche limit crossing parameter space for systems after the first (or only) SN. Considering equation (31) we show the pre- and post-SN parameters. Marked in grey shade are systems that crossed the SMBH Roche limit and thus, unbind the binary are potential LISA events. We denote in the bottom of each panel the corresponding Monte Carlo simulation used. Not that this is a plot only for the Monte Carlo for both a_1 and a_2.

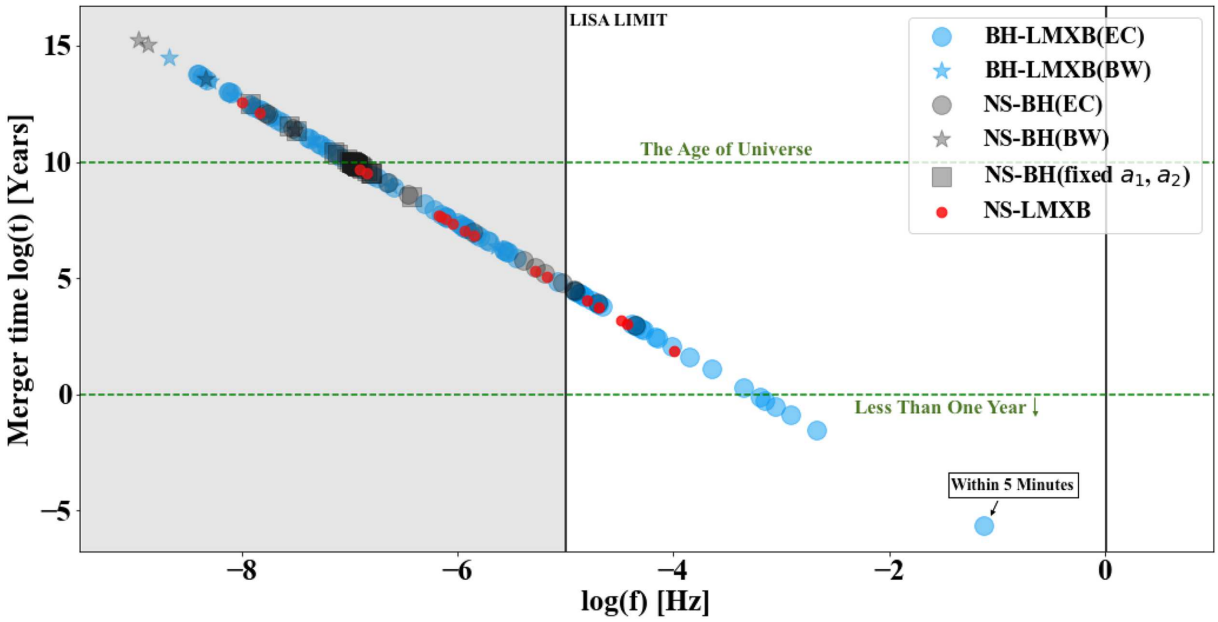

Figure 8. EMRI GW merger time after SN versus GW emission characteristic frequency. We consider all systems in our proof-of-concept Monte Carlo (see below for details) that crossed the SMBH Roche limit (see equation 31). The GW characteristic frequency is computed according to equation (33). The black varietal lines are LISA frequency detection limits. See Table 1 for the fraction of these systems from each Monte Carlo. We note that the systems depicted here are only for the 5 $R_\odot$ runs. The 5 au runs all resulted in longer than Gyr time-scale.

Table 3. Relevant GW merger time with SMBH following one supernova and undergoing Hills process.

Name	Sim	$t_{\rm gw}$ (yr) crossed SMBH $R_{\rm Roche}$
NS–LMXB	(b)	a few (∼1–10) Myr
BH–LMXB	(e)	a few Myr
NS–BH	(j)	a few Myr
		1st SN $t_{\rm gw}$ | 2nd SN $t_{\rm gw}$
NS–NS	(n),(o)	10^{10} | ∼ a few hundred years
BH–BH	(r), (s)	∼ Myr | ∼ h

a_2^{-2} (e.g. Bahcall & Wolf 1976), between $a_2 = 100$ AU and $a_2 = 0.1$ pc. The other orbital parameters were chosen as explained above (see the beginning of Section 4).

Fig. 9 depicts the retention numbers of BH–BH binaries and triples after each of the SN took place (BH–BH are represented in black lines). As shown, large kicks yield larger escape velocities that result in unbinding the binary and triple systems. The fraction of bound binaries after the first SN explosion is of course independent of the mass of the tertiary. However, the fraction of triples that remain bound after the first SN is different. As expected, the triple configuration is more likely to survive with an SMBH as the third companion after the first SN. Specifically, for BH–BH with fixed outer SMA at 1000 AU, only 15 out of 10 000 triple systems remain bound with a stellar tertiary and 4665 with SMBH. For BH–BH binary system, upon first SN, nearly 50 per cent of binaries escape from their stellar companion. When the second SN took place about 0 and 32 per cent of the systems remain bound in the triple configuration with a stellar and SMBH companion, respectively. About 98 per cent of BH–BH binary systems stay bound in a triple system with an SMBH companion, following two SN kicks as large as the ones expected to take place in NS. The kicks expected to take place in BH–BH systems are typically much lower or not at all (see above discussion). Thus, this result suggests that the fraction of BH–BH binaries to exist near Galactic nuclei is rather large, which later can merge via GW emission (e.g. Hoang et al. 2018). We estimate the GW time-scale at which these binaries will merge (see Fig. 10), in the absence of EKL mechanism and find an average merging time of ∼ 1 Myr and reduce to an extremely short time-scale $\sim 10^{-2}$ yr after 2SN and thus resulting in the merger of BH–SMBH detectable by LISA with an SN progenitor.

As mentioned in Appendix E, we also considered a wider initial inner binary ($a_1 = 5$ au). These wider initial systems increase the percentages of systems that cross the stellar (SMBH) companion Roche limit. For example, we consider run (s) for $a_1 = 5\,{\rm R}_\odot$ and run (s5) for $a_1 = 5$ au that represent a BH binary at 1000 au around an SMBH. The tighter initial configuration had about 1 per cent of the system crossing the SMBH Roche limit while the wider resulted in ∼54 per cent (see Tables 1 and E1). Specifically we consider post the first SN (Fig. E2) and after the second SN (Fig. E3). We also present the histogram post the two SNs of these systems (Fig. E1).

4.1.3 *Double neutron star–two natal kicks*

Recently LIGO detected a GW signal from an NS–NS merger (Abbott et al. 2017b) and its associated electromagnetic counterpart (e.g. Abbott et al. 2017c; Alexander et al. 2017; Blanchard et al. 2017; Chornock et al. 2017; Coulter et al. 2017; Fong et al. 2017; Margutti et al. 2017; Nicholl et al. 2017; Soares-Santos et al. 2017). This detection was long expected (e.g. Acernese et al. 2008; Abbott et al. 2009; Somiya 2012) in light of the expected abundance of NS binaries. There are currently about 70 NS binary (or Double NS) systems detected (e.g. Lattimer 2012; Özel & Freire 2016) out of thousands of known NSs (e.g. Hobbs et al. 2005; Manchester et al. 2005). Double NSs are the prime candidate progenitors for short gamma-ray burst events (e.g. Eichler et al. 1989; Metzger et al. 2015) and are also the main candidate for heavy r-process nucleosynthesis sources (e.g. Lattimer & Schramm 1974; Eichler et al. 1989; Beniamini & Piran 2016; Beniamini, Hotokezaka & Piran 2016). The recent detection of GW170817 GW from the coalescence of double NS combined with gamma-ray burst (GRB 170817A) with subsequent ultraviolet, optical, infrared observations (Abbott et al. 2017b) showed that these theoretical models are very promising. Furthermore, Abbott et al. (2016d) placed an upper limit on the merger rate to be $12\,600\,{\rm Gpc}^{-3}\,{\rm yr}^{-1}$. NS binaries (for initially circular systems) have a substantial probability of getting disrupted when one of the stars goes through an SN, either because the instantaneous mass-loss associated with the SN or because of the resulting asymmetry in the imprinted natal kick of the newborn NS.

To explore kicks in NS binary in a triple configuration, we adopt a nominal proof-of-concept system composed with $m_1 = 4\,{\rm M}_\odot$, which leaves an NS with $m_{1,n} = 1.4\,{\rm M}_\odot$, and $m_2 = 5\,{\rm M}_\odot$, which leaves an NS with $m_{2,n} = 1.4\,{\rm M}_\odot$, and $a_1 = 5\,{\rm R}_\odot$, $a_2 = 1000$ AU. As usual, we had two choices for m_3; in the first we set $m_3 = 3\,{\rm M}_\odot$ assuming a stellar companion and in the second we assume that the NS–NS binary is located in the Galactic centre and set $m_3 = 4 \times 10^6\,{\rm M}_\odot$.

For this numerical example [case (n)] we adopt *two* SN natal kicks with each NS. Each SN kick is adopted with the same normal distribution described in Section 4.1.1. As expected the second SN kick significantly reduces the fraction of survived binaries and triples as depicted with red lines in the right-hand panel of Fig. 9 compared to the left-hand panel (1SN), as we see that both dotted and solid red curves have smaller overall amplitudes. In fact, we find that non of our proof-of-concept NS–NS binaries with *stellar* companion remained in triple configuration [as of case(l) and (m)]. That is not surprising as we choose a less massive tertiary ($m_3 = 3\,{\rm M}_\odot$). Again, the triple configuration is more likely to remain bound in the presence of a massive tertiary. Compared to the stellar tertiary that is not able to keep any triple systems bound, we see 20 per cent of triples remains bound out of binaries with an SMBH companion [e.g. see comparison between case (i) and (o) in Table 1]. An SMBH companion will keep a large fraction of the binaries remaining in their triple configuration, which is somewhat sensitive to the outer orbit initial separation (see Table 1). In our test of Bahcall–Wolf distribution [case (n)] we found that about 57 per cent of all survived binaries escaped the system. Thus according to our definition, 6 per cent of these systems will become hypervelocity binaries. We also note that a change in the initial tight inner binary SMA a_1 from $5R_\odot$ to 5 AU would dramatically change the percentage of survived binaries systems with stellar (SMBH) companion crossed the Roche limit of tertiary BH. In the most dramatic case, the percentage change from 3 per cent to ∼84 per cent [see Table E1 case (o) and (o5) post first SN].

We also calculate the merger time via GW emission of the two NS following the kicks and find that for these proof-of-concept initial conditions, after the first SN, the GW merger time is on average longer than the age of the Universe. However, after the second SN, the merging time is relatively short, on average takes 200 yr to merge via GW (as depicted in Fig. 11).

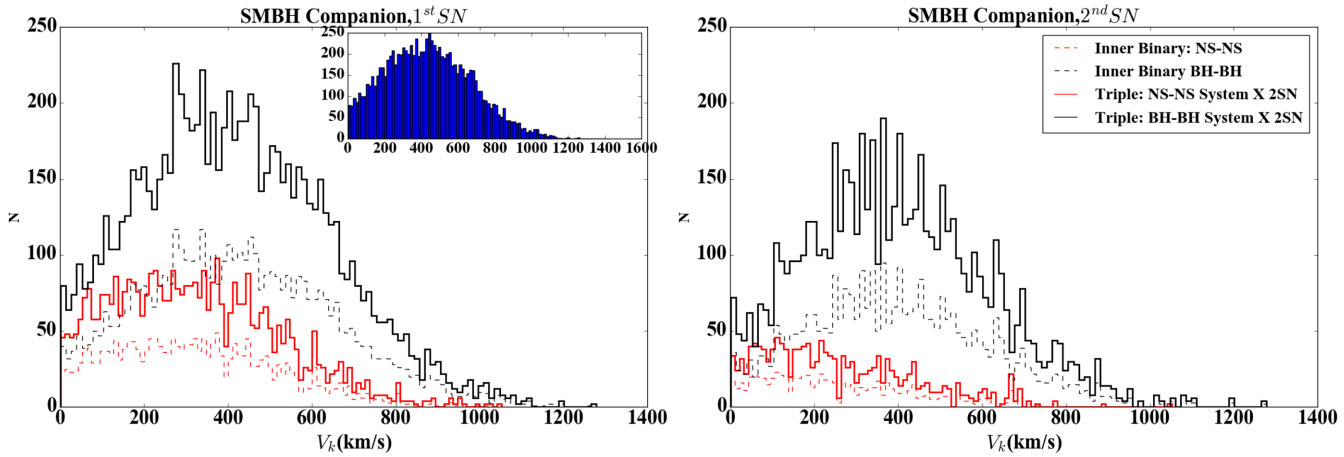

Figure 9. Two natal kicks case. Kick velocity distribution of survived system in GW sources after the *first* SN (left) and the *seconds* SN (right) took place for BH–BH (black lines) and NS–NS (red lines) systems. We consider systems around an SMBH, with $a_1 = 5\,\mathrm{R}_\odot$ and a_2 from $\mathrm{MC}^{2,\,\mathrm{BW}}$, corresponding to runs (n) and (r). We show the surviving binaries (dashed lines) and the surviving triples (solid lines) in each case. The inset shows the initial kick velocity distribution.

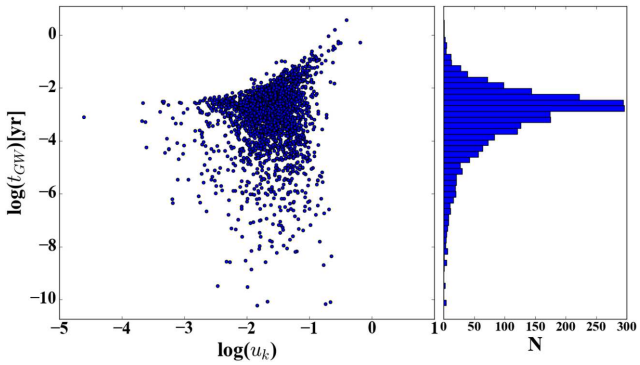

Figure 10. BH–BH GW time-scale after two SNs in systems around SMBH third companion with $a_1 = 5\,\mathrm{R}_\odot$ and a_2 from $\mathrm{MC}^{2,\,\mathrm{BW}}$, i.e. run (r). *Left-hand panel*: We show the GW time-scale as a function of the dimensionless kick velocity, u_k. In the *right-hand panel* we show the histogram of the GW time-scales.

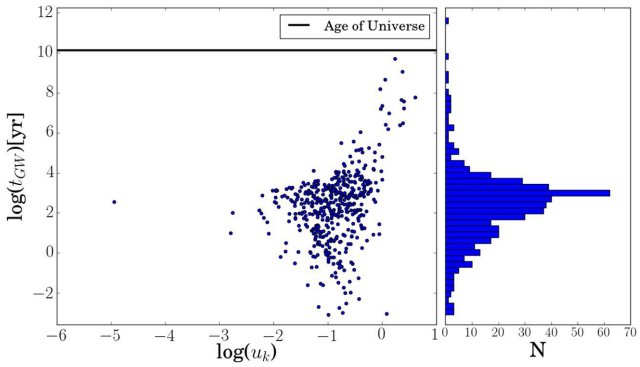

Figure 11. NS–NS GW time-scale after two SNs in systems around SMBH third companion with $a_1 = 5\,\mathrm{R}_\odot$ and a_2 from $\mathrm{MC}^{2,\mathrm{BW}}$, i.e. run (n). *Left-hand panel*: We show the GW time-scale as a function of the dimensionless kick velocity, u_k. In the *right-hand panel* we show the histogram of the GW time-scales.

We note that Michaely & Perets (2018) found that in some cases, the SN kick caused the NS–NS systems to reach such small separations that they cross the Roche limit or even immediately merge via GW emission. Since in our numerical experiments, we have made sure to place the tertiary far away such that $\varepsilon < 0.1$; on average the GW emission will have about 200 yr delay, while a small fraction of them will have only few days (and as low as few hours) delay (see Fig. 11).

4.2 Low-mass X-ray binaries

A substantial number of close binaries with an accreting compact object, mainly low-mass X-ray binaries (LMXBs) and their descendants (i.e. millisecond radio pulsars) are known or suspected triples (Bailyn & Grindlay 1987; Grindlay et al. 1988; Garcia 1989; Thorsett, Arzoumanian & Taylor 1993; Corbet et al. 1994; Thorsett et al. 1999; Chou & Grindlay 2001; Rasio 2001; Sigurdsson et al. 2003; Zdziarski, Wen & Gierliński 2007; Prodan & Murray 2012). Furthermore, it was recently suggested that the inner 1 pc of the Galactic centre host an over abundance of X-ray binaries (e.g. see Hailey et al. 2018) Thus, a natural question is what is the probability that these systems will remain in their triple configuration after the SN natal kick took place.

In each case of BH- and NS-LMXB we have three Monte Carlo tests. In all we choose a_1 from a Monte Carlo simulation labelled MC^1 that is uniform in log between $5\,\mathrm{R}_\odot$ and a $1000\,\mathrm{R}_\odot$. We also choose a_2 to follow either $\mathrm{MC}^{2,\mathrm{EC}}$ (consistent with a_2^{-3}), or $\mathrm{MC}^{2,\mathrm{BW}}$ (consistent with a_2^{-2}; e.g. Bahcall & Wolf 1976). As before we have two masses for the third companion, stellar companion with $3\,\mathrm{M}_\odot$ and an SMBH with $4 \times 10^6\,\mathrm{M}_\odot$ (see Table 1 for more information). We chose the inner and outer orbital eccentricity from a uniform distribution (e.g. Raghavan et al. 2010), and the mutual inclination is chosen from an isotropic distribution (i.e. uniform in $\cos i$). In addition, the inner and outer argument of periapsis angles are chosen from a uniform distribution between $0 - 2\pi$.

4.2.1 Neutron star low-mass X-ray binaries

In this case, we adopt a nominal system composed of $m_1 = 1\,\mathrm{M}_\odot$, $m_2 = 4\,\mathrm{M}_\odot$, which leaves an NS with $m_{2,\,n} = 1.4\,\mathrm{M}_\odot$. We have tested three simplified Monte Carlo runs (see Table 1) and

found that only 4 per cent of all binaries remain bound after the kick, for both SMBH and stellar third companion. Considering the stellar tertiary proof-of-concept test, i.e. run (a), we found that the SN kicks disrupt all of the stellar triples. Considering an SMBH triple companion [runs (b) and (c)], we find that 94 per cent and 99 per cent, respectively, out of the surviving binaries will stay bound to the SMBH companion (see Fig. 12). The remaining binaries will escape the SMBH potential well at velocity smaller than 200 km s^{-1}.

In addition, we found that 19 per cent of all survived binary systems cross the low-mass star Roche limit and start accreting on to the NS. In other words $a_{1,n}(1-e_{1,n}) \leq R_{\rm Roche}$, and

$$R_{\rm Roche} = 1.6 R_\star \left(\frac{m_\star}{m_{NS}+m_\star}\right)^{-1/3}, \quad (34)$$

where $R_\star$ is the radius of the star. These systems are forming NS–LMXB immediately after the SN.

We also found that 4 per cent out of the triples systems crossed the tertiary SMBH companion's Roche limit according to equation (31). In the case of SMBH tertiary, these NSs will merge with the SMBH by emitting GWs after about an Myr on average. Thus, producing a GW–LISA event with a possible young SN remnant.

4.2.2 *Black hole low-mass X-ray binaries*

The formation of BH–LMXB poses a theoretical challenge as low-mass companions are not expected to survive the common-envelope scenario with the BH progenitor (see Podsiadlowski, Rappaport & Han 2003). Recently, Naoz et al. (2016) proposed a new formation mechanism that skips the common-envelope scenario and relies on triple-body dynamics. Specifically, using the EKL mechanism (e.g. Naoz 2016), they showed that eccentricity excitations due to gravitational perturbations from a third star can rather efficiently form BH–LMXB. Their calculations assume no SN kicks, consistent with the observational and theoretical studies (e.g. Willems et al. 2005; Reid et al. 2014; Ertl et al. 2016; Mandel 2016; Sukhbold et al. 2016). However, at least in one system robust evidence for a non-negligible natal kick imparted on to a BH system was detected (e.g. Gualandris et al. 2005; Fragos et al. 2009). Here we show that even given large SN kicks in these systems, it still allows for large fraction of these systems to remain bound.

We adopt a nominal system of $m_1 = 1\,{\rm M}_\odot$, $m_2 = 9\,{\rm M}_\odot$ that leaves a BH with a mass of $m_{2,n} = 7\,{\rm M}_\odot$ (which follows the stellar evolution adopted from *SSE* code; Hurley et al. 2000). We chose our orbital parameters as explained above. The kick magnitude distribution was chosen in the same way as described above (see Section 4.2.1). We find that about 11 per cent of the binaries survived (as depicted in Fig. 12). For BH–LMXB with stellar mass companion, we found 11 per cent of binaries (out of all 99 per cent) escape from its stellar companion at hypervelocity. Furthermore, we find that about 1 per cent of the surviving binaries remained in their triple configurations for stellar mass companions and as expected 99 per cent for the SMBH companion. Not surprisingly, this is a larger fraction than the surviving NS–LMXB triple system as (i) the BH mass has a larger gravitational potential and (ii) the mass-loss was substantially a smaller fraction of the initial mass compared to the NS explosion. Thus, we find that Naoz et al. (2016) BH–LMXB mechanism can still work even in the presence of large natal SN kicks for the BH.

In our simulations we found that ∼24 per cent of all binaries cross their Roche limits (see equation 34) and thus form BH–LMXB. We also found that ∼13 per cent of all triples cross the stellar third companion's Roche limits according to equation (31), again forming BH–LMXB, immediately after the SN.

In the case of binaries around SMBH, we found that in 7 per cent of triple systems, the newly formed stellar mass BH crosses the SMBH Roche limit, thus merging with the SMBH on a typical time-scale of 10 Myr and can be as short as few minutes (see Fig. 8). This potentially forms a system detectable by LISA after the SN, thus allowing for an optical precursor counterpart appearing shortly before the GW detection.

5 DISCUSSION

We analysed SN kicks in triple configurations. In recent years, hierarchical triple body have been proven to be very useful in addressing and understanding the dynamics of various systems from exoplanets to triple stars and compact object systems (see Naoz 2016, and references therein). As a star undergoes SN and forms an NS (or BH), it is expected to have a natal kick. In a binary system, this kick may cause the velocity vector orientation and amplitude of the mutual centre of mass to vary. The consequences of such a kick in a *binary* system has been previously investigated in the literature, often focused on circular orbits. With the gaining interest in triple systems, we address the natal kick consequences in the context of triple systems with eccentric orbits.

We have derived the analytical equations that describe the effect of a natal kick in hierarchical triple body systems. Triple systems have been considered in the literature as a promising mechanism to induce compact object binaries through GW emissions (e.g. Blaes et al. 2002; Antonini et al. 2010; Thompson 2011; Pijloo et al. 2012; Michaely et al. 2016; VanLandingham et al. 2016; Petrovich & Antonini 2017; Silsbee & Tremaine 2017; Hamers et al. 2018; Hoang et al. 2018; Randall & Xianyu 2018a; Randall & Xianyu 2018b). We consider the effects of SN kick in keeping compact object binaries and triples on bound orbits. Furthermore, we also consider the effects of kicks in producing LMXB.

We have run proof-of-concept Monte Carlo simulations to test the range of applications of SN kicks in hierarchical triples. Below we summarize our significant results.

(i) **SN kicks may shrink the binary SMA.** We pointed out that SN kicks can lead the binary SMA to *shrink* in many cases, as can be seen from equation (23). See, for example, Fig. 5 for the agreement between the analytical and numerical results for the shrinking condition. In fact, we found that a combination of expanding of the inner orbit and shirking of the outer orbit cause a non-negligible fraction of our systems to cross the inner binary's Roche limit as well as the outer orbit's Roche limit, resulting in destruction of the triple system and a possible merger with the tertiary companion. Shrinking the inner orbit binary SMA can trigger a merger or a common envelope event. Crossing the tertiary's Roche limit has far more dramatic consequences as we elaborate below.

(ii) **Massive tertiaries**. As expected, we find that the triple configuration remains bound when the tertiary is more massive (see Fig. 3 and compare the right-hand and left-hand panels in Figs 4, 9, and 12). This trend has significant implications on the formation of LMXBs as well as GW emission from compact objects.
Naoz et al. (2016) recently suggested that gravitational perturbations from a distant companion can facilitate the formation of LMXBs, thus overcoming the nominal theoretical challenge associated with the BH–LMXB formation, since low-mass companions are not expected to survive the common-envelope phase with the BH

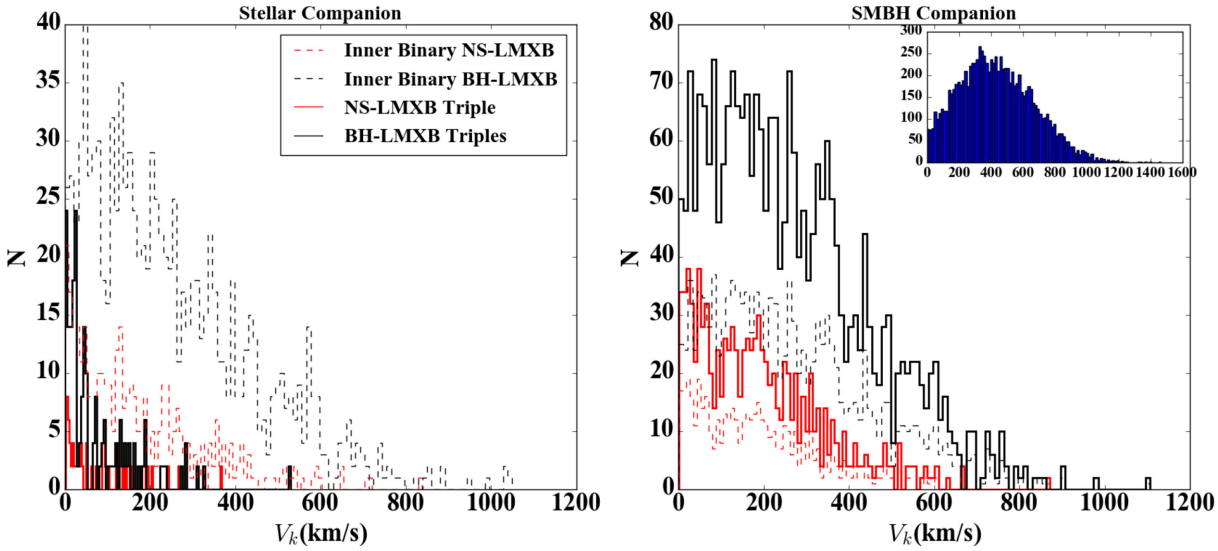

Figure 12. Kick velocity distribution of survived system in BH–LMXB (black lines), NS–LMXB (red lines) with an SMBH companion. This is for systems with a_1 chosen from MC[1] and a_2 from MC[2,EC]. In the *left-hand panel* we consider a stellar companion as the tertiary $3\,M_\odot$ while in the *right-hand panel* we consider $4 \times 10^6\,M_\odot$ companion. We show the survived binary distribution for the systems in dashed lines while the solid lines depict the distribution of the survived triple systems. The initial distribution (identical in both bases) is depicted in the inset.

progenitor. Therefore, our result that the majority of binaries remain near an SMBH post SN kick (e.g. Fig. 12) suggests that SMBH environment yields a larger abundance of LMXBs.

Furthermore, the SMBHs gravitational perturbations can enhance the compact objects merger rate (e.g. Antonini et al. 2014), which can result in a non-negligible rate from $1-14\,\mathrm{Gpc^{-3}\,yr^{-1}}$ (Hoang et al. 2018). Our results here suggest that the majority of binaries that survive the SN kick will not escape the SMBH potential wells as expected.

(iii) **Hypervelocity binaries**. When the tertiary companion is a star, the SN kick tends to simply disrupt triple stellar system. However, if the tertiary is an SMBH an SN kick leads to a few per cent of the binaries escaping the SMBH potential well and will be observed as hypervelocity binary system.

(iv) **Simultaneous and precursors electromagnetic signatures for LIGO compact object merger event.** We find that since the SN kick can shrink the SMA of the binary orbit, it leads to a short GW emission merging time, which will be prompted by SN. This type of behaviour was pointed out previously by Michaely & Perets (2018) for inner binaries. We find similar results, for our NS–BH, BH–BH, and NS–NS proof-of-concept examples (e.g. Figs 6, 10, and 11). Consistently with Michaely & Perets (2018), we find that many of these LIGO events will have an SN remnant signature. Furthermore, for the systems that underwent two SN kicks, we find that the SN can be either as a precursors or even almost simultaneous with the GW detection. For example, as shown in Fig. 10, for BH–BH merger, on average, the SN precursor takes place about a month before the GW detection, with some that will take place almost instantaneously.

(v) **Electromagnetic precursors for LISA events.** Finally, we find that the SN kick causes a non-negligible fraction of the systems near an SMBH to cross the SMBH Roche limit. If the companion star crosses the Roche limit of SMBH, it will cause a tidal disruption event TDE, shortly after the SN. Interestingly, if the compact object crossed the SMBH Roche limit, resulting an EMRI. Thus, we find that GW emission might result in a LISA event after a wide range of times, which depends on the Monte Carlo configuration. On average, events in the LISA detection band will take place about a few Myr after the SN, and they can be as quick as a few minutes after the SN explosion.

We have tested a wide range of initial conditions, from a tight binary ($a_1 = 5\,R_\odot$, which represents most of the discussion throughout the paper) to a wide initial binary ($a_1 = 5$ au, see Appendix E). The former may represent a stable binary that survived a common-envelope evolution. In both cases, the qualitative result seems to hold, but the fraction, as expected differs. For example, the fraction of binaries that survive SN kick diminishes, but the fraction of systems that crossed the tertiary Roche limit goes up. The latter is especially interesting, as it can cause either a TDE or an EMRI with a possible SN precursor.

ACKNOWLEDGEMENTS

We thank the referee for a thoughtful read of the paper and comments that helped strengthen our paper. We thank Alexander Stephan and Bao-Minh Hoang for useful discussion and suggestions. CL acknowledges the UCLA Van Tree Foundation, Undergraduate Research Scholars Program Scholarship as well as the Stone Foundation Summer Research Scholarship. CL thanks Izuki Matsuba for discussion and help. SN acknowledges the partial support of the Sloan fellowship and from the NSF through grant No. AST-1739160.

REFERENCES

Abbott B. P. et al., 2009, Rep. Prog. Phys., 72, 076901
Abbott B. P. et al., 2016a, Phys. Rev. X, 6, 041015
Abbott B. P. et al., 2016b, Phys. Rev. D, 93, 122003
Abbott B. P. et al., 2016c, Phys. Rev. Lett., 116, 241103
Abbott B. P. et al., 2016d, ApJ, 832, L21
Abbott B. P. et al., 2017a, Phys. Rev. Lett., 119, 161101
Abbott B. P. et al., 2017b, ApJ, 848, L12
Abbott B. P. et al., 2017c, ApJ, 848, L12
Acernese F. et al., 2008, Class. Quantum Gravity, 25, 114045
Alexander K. D. et al., 2017, ApJ, 848, 69

Antognini J. M., Shappee B. J., Thompson T. A., Amaro-Seoane P., 2014, MNRAS, 439, 1079
Antonini F., Faber J., Gualandris A., Merritt D., 2010, ApJ, 713, 90
Antonini F., Murray N., Mikkola S., 2014, ApJ, 781, 45
Arzoumanian Z., Chernoff D. F., Cordes J. M., 2002, ApJ, 568, 289
Bahcall J. N., Wolf R. A., 1976, ApJ, 209, 214
Bahcall J. N., Wolf R. A., 1977, ApJ, 216, 883
Bailyn C. D., Grindlay J. E., 1987, ApJ, 316, L25
Belczynski K., Sadowski A., Rasio F. A., Bulik T., 2006, ApJ, 650, 303
Beniamini P., Piran T., 2016, MNRAS, 456, 4089
Beniamini P., Hotokezaka K., Piran T., 2016, ApJ, 829, L13
Blaes O., Lee M. H., Socrates A., 2002, ApJ, 578, 775
Blanchard P. K. et al., 2017, ApJ, 848, L22
Bode J. N., Wegg C., 2014, MNRAS, 438, 573
Borkovits T., Hajdu T., Sztakovics J., Rappaport S., Levine A., Bíró I. B., Klagyivik P., 2016, MNRAS, 455, 4136
Bortolas E., Mapelli M., Spera M., 2017, MNRAS, 469, 1510
Chornock R. et al., 2017, ApJ, 848, L19
Chou Y., Grindlay J. E., 2001, ApJ, 563, 934
Corbet R. H. D., Asai K., Dotani T., Nagase F., 1994, ApJ, 436, L15
Cordes J. M., Chernoff D. F., 1998, ApJ, 505, 315
Coulter D. A. et al., 2017, Science, 358, 1556
Dominik M., Belczynski K., Fryer C., Holz D. E., Berti E., Bulik T., Mandel I., O'Shaughnessy R., 2012, ApJ, 759, 52
Eggleton P. P., Kisseleva-Eggleton L., Dearborn X., 2007, in Hartkopf W. I., Guinan E. F., Harmanec P., eds, IAU Symposium Vol. 240, Binary Stars as Critical Tools & Tests in Contemporary Astrophysics. Cambridge Univ. Press, Cambridge, p. 347
Eichler D., Livio M., Piran T., Schramm D. N., 1989, Nature, 340, 126
Ertl T., Janka H.-T., Woosley S. E., Sukhbold T., Ugliano M., 2016, ApJ, 818, 124
Faucher-Giguère C.-A., Loeb A., 2011, MNRAS, 415, 3951
Fong W. et al., 2017, ApJ, 848, L23
Fragos T., Willems B., Kalogera V., Ivanova N., Rockefeller G., Fryer C. L., Young P. A., 2009, ApJ, 697, 1057
Fryer C. L., Woosley S. E., Hartmann D. H., 1999, ApJ, 526, 152
Garcia M. R., 1989, in Hunt J., Battrick B., eds, ESA Special Publication Vol. 296, Two Topics in X-Ray Astronomy, Volume 1: X-Ray Binaries. Volume 2: AGN and the X-Ray Background. European Space Agency, Paris.
Gillessen S. et al., 2012, Nature, 481, 51
Grindlay J. E., Bailyn C. D., Cohn H., Lugger P. M., Thorstensen J. R., Wegner G., 1988, ApJ, 334, L25
Gualandris A., Colpi M., Portegies Zwart S., Possenti A., 2005, ApJ, 618, 845
Hailey C. J., Mori K., Bauer F. E., Berkowitz M. E., Hong J., Hord B. J., 2018, Nature, 556, 70
Hamers A. S., 2018, MNRAS, 476, 4139
Hamers A. S., Pols O. R., Claeys J. S. W., Nelemans G., 2013, MNRAS, 430, 2262
Hamers A. S., Bar-Or B., Petrovich C., Antonini F., 2018, ApJ, 865, 2
Hansen B. M. S., Phinney E. S., 1997, MNRAS, 291, 569
Hills J. G., 1983, ApJ, 267, 322
Hills J. G., 1988, Nature, 331, 687
Hirai R., Podsiadlowski P., Yamada S., 2018, ApJ, 864, 119
Hoang B. M., Naoz S., Kocsis B., Rasio F. A., Dosopoulou F., 2018, ApJ, 856, 140
Hobbs G., Lyne A. G., Kramer M., Martin C. E., Jordan C., 2004, MNRAS, 353, 1311
Hobbs G., Lorimer D. R., Lyne A. G., Kramer M., 2005, MNRAS, 360, 974
Hurley J. R., Pols O. R., Tout C. A., 2000, MNRAS, 315, 543
Hurley J. R., Tout C. A., Pols O. R., 2002, MNRAS, 329, 897
Ivanov P. B., Polnarev A. G., Saha P., 2005, MNRAS, 358, 1361
Kalogera V., 1996, ApJ, 471, 352
Kalogera V., 2000, ApJ, 541, 319
Kalogera V., Kolb U., King A. R., 1998, ApJ, 504, 967
Kaspi V. M., Bailes M., Manchester R. N., Stappers B. W., Bell J. F., 1996, Nature, 381, 584
Katz B., Dong S., 2012, preprint (arXiv:1211.4584)
Kiel P. D., Hurley J. R., 2009, MNRAS, 395, 2326
Lai D., Bildsten L., Kaspi V. M., 1995, ApJ, 452, 819
Lattimer J. M., 2012, Annu. Rev. Nucl. Part. Sci., 62, 485
Lattimer J. M., Schramm D. N., 1974, ApJ, 192, L145
LIGO Scientific Virgo Collaboration, 2017, Phys. Rev. Lett., 118, 221101
Lithwick Y., Naoz S., 2011, ApJ, 742, 94
Lorimer D. R., Bailes M., Harrison P. A., 1997, MNRAS, 289, 592
Lu J. R., Do T., Ghez A. M., Morris M. R., Yelda S., Matthews K., 2013, ApJ, 764, 155
Manchester R. N., Hobbs G. B., Teoh A., Hobbs M., 2005, AJ, 129, 1993
Mandel I., 2016, MNRAS, 456, 578
Mardling R. A., Aarseth S. J., 2001, MNRAS, 321, 398
Margutti R. et al., 2017, ApJ, 848, L20
Martins F. et al., 2006, ApJ, 649, L103
Metzger B. D., Margalit B., Kasen D., Quataert E., 2015, MNRAS, 454, 3311
Michaely E., Perets H. B., 2014, ApJ, 794, 122
Michaely E., Perets H. B., 2018, ApJ, 855, L12
Michaely E., Ginzburg D., Perets H. B., 2016, preprint (arXiv:1610.00593)
Murray C. D., Dermott S. F., 2000, Solar System Dynamics. Cambridge Univ. Press, Cambridge
Mylläri A., Valtonen M., Pasechnik A., Mikkola S., 2018, MNRAS, 476, 830
Naoz S., 2016, ARA&A, 54, 441
Naoz S., Silk J., 2014, ApJ, 795, 102
Naoz S., Farr W. M., Lithwick Y., Rasio F. A., Teyssandier J., 2013, MNRAS, 431, 2155
Naoz S., Fragos T., Geller A., Stephan A. P., Rasio F. A., 2016, ApJ, 822, L24
Naoz S., Ghez A. M., Hees A., Do T., Witzel G., Lu J. R., 2018, ApJ, 853, L24
Nicholl M. et al., 2017, ApJ, 848, L18
Ott T., Eckart A., Genzel R., 1999, ApJ, 523, 248
Parker R. J., 2017, in Alsabti A., Murdin P., eds, Handbook of Supernovae: the Effects of Supernovae on the Dynamical Evolution of Binary Stars and Star Clusters. Springer, Cham, p. 2313
Perets H. B., Kratter K. M., 2012, ApJ, 760, 99
Peters P. C., 1964, Phys. Rev., 136, 1224
Peters P. C., Mathews J., 1963, Phys. Rev., 131, 435
Petrovich C., 2015, ApJ, 808, 120
Petrovich C., Antonini F., 2017, ApJ, 846, 146
Pfahl E., Podsiadlowski P., Rappaport S., 2005, ApJ, 628, 343
Pfuhl O., Alexander T., Gillessen S., Martins F., Genzel R., Eisenhauer F., Fritz T. K., Ott T., 2014, ApJ, 782, 101
Pijloo J. T., Caputo D. P., Portegies Zwart S. F., 2012, MNRAS, 424, 2914
Podsiadlowski P., Rappaport S., Han Z., 2003, MNRAS, 341, 385
Portegies Zwart S. F., Baumgardt H., McMillan S. L. W., Makino J., Hut P., Ebisuzaki T., 2006, ApJ, 641, 319
Postnov K. A., Yungelson L. R., 2014, Living Rev. Relativ., 17, 3
Press W. H., Thorne K. S., 1972, ARA&A, 10, 335
Pribulla T., Rucinski S. M., 2006, AJ, 131, 2986
Prodan S., Murray N., 2012, ApJ, 747, 4
Rafelski M., Ghez A. M., Hornstein S. D., Lu J. R., Morris M., 2007, ApJ, 659, 1241
Raghavan D. et al., 2010, ApJS, 190, 1
Randall L., Xianyu Z.-Z., 2018a, ApJ, 853, 93
Randall L., Xianyu Z.-Z., 2018b, ApJ, 864, 134
Rasio F. A., 2001, in Podsiadlowski P., Rappaport S., King A. R., D'Antona F., Burderi L., eds, ASP Conf. Ser. Vol. 229, Evolution of Binary and Multiple Star Systems: A Meeting in Celebration of Peter Eggleton's 60th Birthday. Astron. Soc. Pac., San Francisco, p. 117
Reid M. J., McClintock J. E., Steiner J. F., Steeghs D., Remillard R. A., Dhawan V., Narayan R., 2014, ApJ, 796, 2
Repetto S., Nelemans G., 2015, MNRAS, 453, 3341
Repetto S., Davies M. B., Sigurdsson S., 2012, MNRAS, 425, 2799
Sana H. et al., 2012, Science, 337, 444
Savransky D., Cady E., Kasdin N. J., 2011, ApJ, 728, 66

Shappee B. J., Thompson T. A., 2013, ApJ, 766, 64
Sigurdsson S., Richer H. B., Hansen B. M., Stairs I. H., Thorsett S. E., 2003, Science, 301, 193
Silsbee K., Tremaine S., 2017, ApJ, 836, 39
Soares-Santos M. et al., 2017, ApJ, 848, L16
Somiya K., 2012, Class. Quantum Gravity, 29, 124007
Stephan A. P., Naoz S., Ghez A. M., Witzel G., Sitarski B. N., Do T., Kocsis B., 2016, MNRAS, 460, 3494
Stephan A. P., Naoz S., Zuckerman B., 2017, ApJ, 844, L16
Stephan A. P., Naoz S., Gaudi B. S., 2018, AJ, 156, 128
Sukhbold T., Ertl T., Woosley S. E., Brown J. M., Janka H.-T., 2016, ApJ, 821, 38
Tauris T. M., 2015, MNRAS, 448, L6
Tauris T. M., Takens R. J., 1998, A&A, 330, 1047
Tauris T. M., van den Heuvel E. P. J., 2014, ApJ, 781, L13
Thompson T. A., 2011, ApJ, 741, 82
Thorsett S. E., Arzoumanian Z., Taylor J. H., 1993, ApJ, 412, L33
Thorsett S. E., Arzoumanian Z., Camilo F., Lyne A. G., 1999, ApJ, 523, 763
Tokovinin A., 2008, MNRAS, 389, 925
Tokovinin A., Hartung M., Hayward T. L., 2010, AJ, 140, 510
Tokovinin A. A., 1997, Astron. Lett., 23, 727
Toonen S., Hamers A., Portegies Zwart S., 2016, Comput. Astrophys. Cosmol., 3, 6
Valtonen M., Karttunen H., 2006, The Three-Body Problem. Cambridge Univ. Press, Cambridge
VanLandingham J. H., Miller M. C., Hamilton D. P., Richardson D. C., 2016, ApJ, 828, 77
Willems B., Henninger M., Levin T., Ivanova N., Kalogera V., McGhee K., Timmes F. X., Fryer C. L., 2005, ApJ, 625, 324
Witzel G. et al., 2014, ApJ, 796, L8
Witzel G. et al., 2017, ApJ, 847, 80
Yu Q., Tremaine S., 2003, ApJ, 599, 1129
Zdziarski A. A., Wen L., Gierliński M., 2007, MNRAS, 377, 1006
Zubovas K., Wynn G. A., Gualandris A., 2013, ApJ, 771, 118
Özel F., Freire P., 2016, ARA&A, 54, 401

APPENDIX A: THE POST-SN ANGULAR MOMENTUM

Opening equation (19)

$$J_1^2 = \frac{1+u_k^2-2\beta+2u_k\cos\theta+e_1\cos E_1(1+u_k^2+2u_k\cos\theta)}{\beta(e_1\cos E_1-1)}\left(1+u_k^2-e_1^2(1+u_k^2)\cos^2 E_1-e_1^2\sin^2 E_1+\frac{1}{2}u_k(-1+e_1\cos E_1)\right.$$
$$\left.\times\left[2u_k(1+e_1\cos E_1)\cos^2\alpha-4(1+e_1\cos E_1)\cos\theta+4e_1\sqrt{\frac{1+e_1\cos E_1}{e_1\cos E_1-1}}\cos\alpha\sin E_1\right]\right) \quad \text{(A1)}$$

APPENDIX B: THE TILT ANGLE

The tilt angle is defined as the angle between the plane of the post-SN orbital plane and the pre-SN plane. Kalogera (2000) studied the tilt angle following an SN kick in a circular binary. The tilt angle can be related to spin–orbit misalignment that can affect their resulted gravitational radiation waveforms of coalescing compact binaries and thus affect their detectability. Using the eccentricity vector

$$\boldsymbol{e} = \frac{1}{\mu}\left(\dot{\boldsymbol{r}}\times\boldsymbol{h}-\mu\frac{\boldsymbol{r}}{r}\right), \quad \text{(B1)}$$

where $\mu = G(m_1+m_2)$, we can find the tilt angle between the post- and pre-SN explosion that we denote as $\Delta\psi$. This angle is simply

$$\cos\Delta\psi_1 = \frac{\boldsymbol{e}_{1,n}\cdot\boldsymbol{e}_1}{e_{1,n}e_1}, \quad \text{(B2)}$$

where $e_{1,n}$ is found using equation (19).

APPENDIX C: POST- AND PRE-SN VELOCITY RELATIONS

The velocity vector to the inner orbit that is associated with $\boldsymbol{r} = \boldsymbol{r}_2 - \boldsymbol{r}_1$ (see Fig. 1) is defined by $\boldsymbol{v}_r = \boldsymbol{v}_2 - \boldsymbol{v}_1$. The velocity vector of the outer orbit is defined by $\boldsymbol{V}_3 = \boldsymbol{v}_3 - \boldsymbol{v}_{\rm c.m.}$, where $\boldsymbol{v}_3$ is the velocity vector associated with the position vector $\boldsymbol{r}_3$ and $\boldsymbol{v}_{\rm c.m.}$ is the velocity vector of the inner orbit centre of mass associated with the centre of mass position vector $\boldsymbol{r}_{\rm c.m.}$ (see Fig. 1). Note that

$$\boldsymbol{v}_{\rm c.m.} = \frac{m_1\boldsymbol{v}_1+m_2\boldsymbol{v}_2}{m_1+m_2}. \quad \text{(C1)}$$

As m_2 undergoes SNe, we find that $\boldsymbol{v}_{r,n} = \boldsymbol{v}_2+\boldsymbol{v}_k-\boldsymbol{v}_1 = \boldsymbol{v}_r+\boldsymbol{v}_k$ and thus the new outer orbit velocity is

$$\boldsymbol{V}_{3,n} = \boldsymbol{V}_3 - \frac{m_1(m_{2,n}-m_2)\boldsymbol{v}_r}{(m_1+m_{2,n})(m_1+m_2)} + \frac{m_{2,n}}{m_1+m_{2,n}}\boldsymbol{v}_k \quad \text{for} \quad m_2\to m_{2,n}. \quad \text{(C2)}$$

Note that if m_1 undergoes SN then

$$\boldsymbol{V}_{3,n} = \boldsymbol{V}_3 - \frac{m_2(m_1-m_{1,n})\boldsymbol{v}_r}{(m_2+m_{1,n})(m_1+m_2)} - \frac{m_{1,n}}{m_2+m_{1,n}}\boldsymbol{v}_k \quad \text{for} \quad m_1\to m_{1,n}. \quad \text{(C3)}$$

Note that all the vectors need to be rotated with respect to the invariable plane.

APPENDIX D: ORBITAL PARAMETER PLOTS FOR THE BH–BH SYSTEM

Motivated by the recent LIGO detection, we provide the orbital parameters distribution of one of our proof-of-concept runs. Specifically, we chose to show the case for which $a_1 = 5\,{\rm R}_\odot$, $a_2 = 1000$ AU, and an SMBH tertiary (see Hoang et al. 2018). This system is shown in Figs E2 and E3.

APPENDIX E: RUNS WITH WIDER INNER BINARY

Here we present a table with the Monte Carlo results while setting $a_1 = 5$ au. To allow comparison we reiterate the nominal results considered throughout the paper. All these runs are noted as *A*5, where *A* is the nominal runs presented in Table 1.

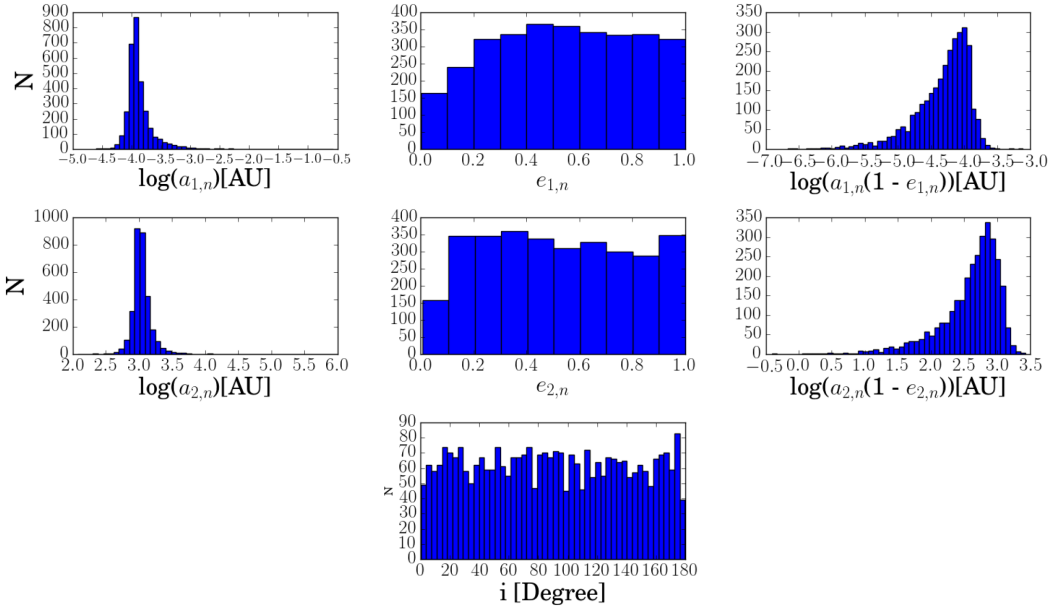

Figure E1. The post-SN for BHB orbital parameters distribution after two SN with tertiary SMBH. BHB system has initial condition of $a_1 = 5\,\mathrm{R}\odot$ and $a_2 = 1000$ AU (see Section 4.1.2 for description of initial conditions and Table 1 for statistics). This system represents a typical system investigated by Hoang et al. (2018).

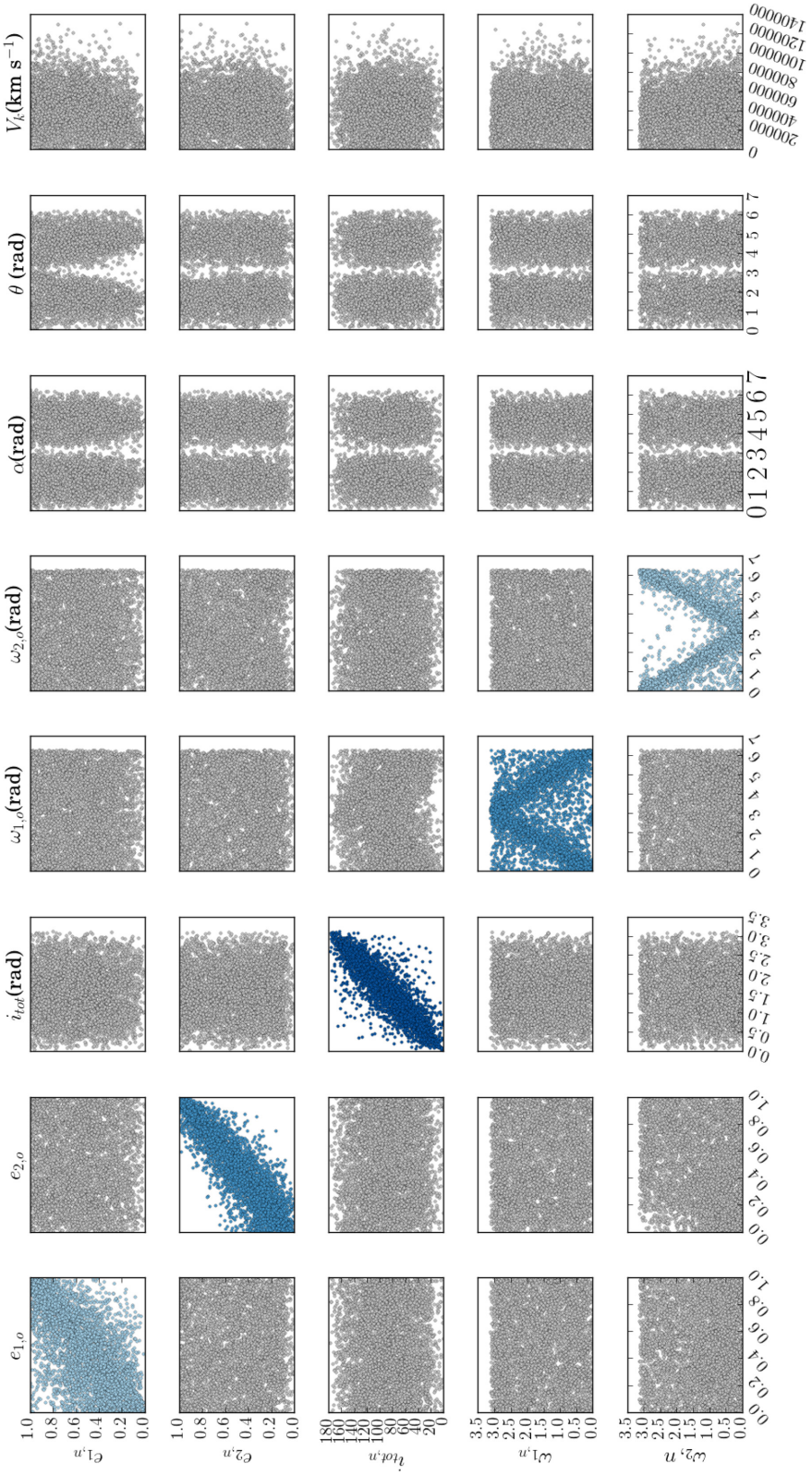

Figure E2. BHB system (with SMBH tertiary) after first SN and its resulting changes in parameters. This is for systems with $a_1 = 5\,\mathrm{R}_\odot$ and $a_2 = 1000\,\mathrm{AU}$. The subscript 'o' means pre-SN orbital parameter values and the subscript 'n' stands for the values of orbital parameters after first SN.

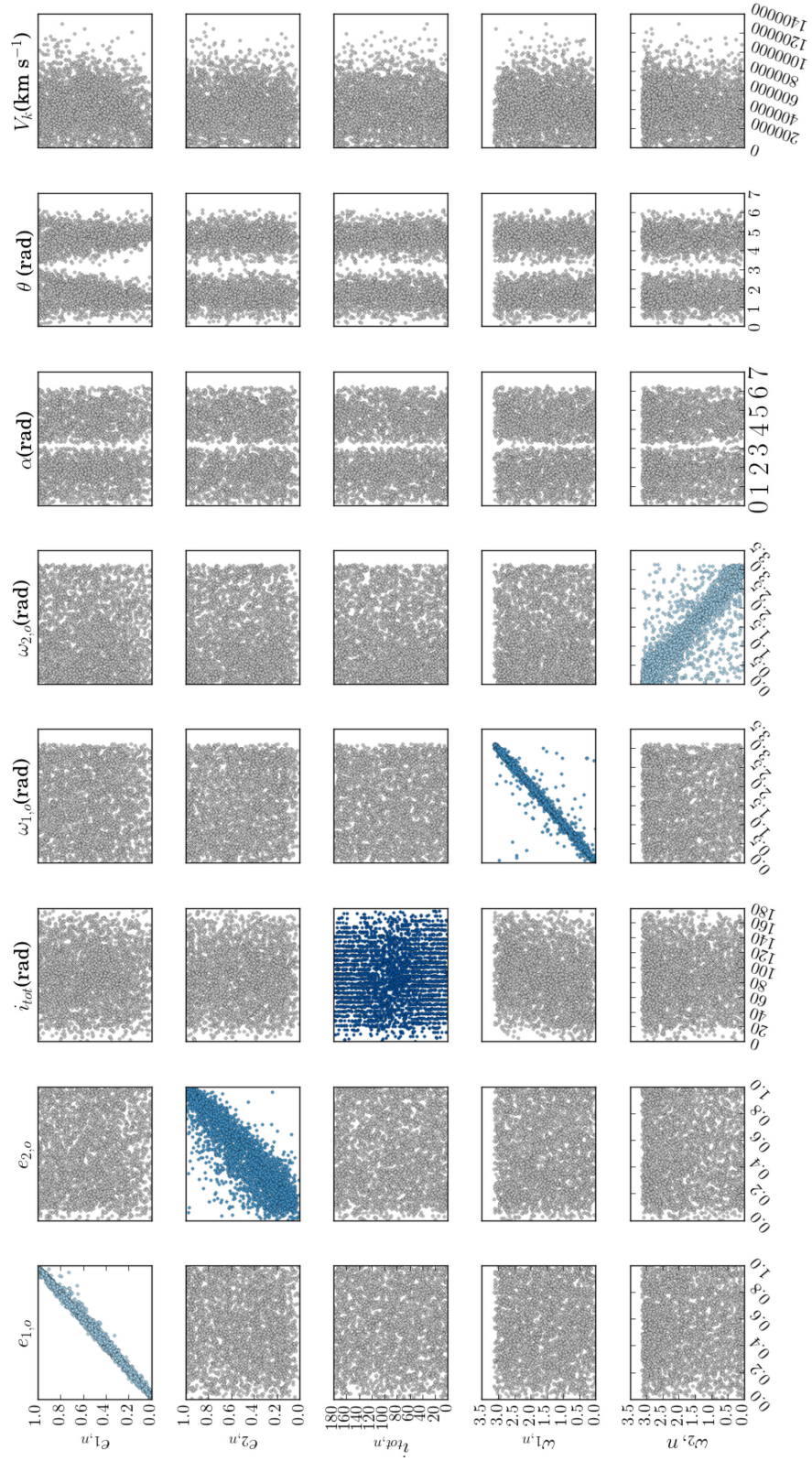

Figure E3. BHB (with SMBH tertiary) system after second SN and its resulting changes in parameters. This is for systems with $a_1 = 5\,\mathrm{R}_\odot$ and $a_2 = 1000$ AU. The subscript 'o' means post-first SN orbital parameter values and the subscript 'n' stands for the values of orbital parameters after second SN.

Table E1. Table of the numerical experiments run below. We show the masses of the inner binary (pre- and post-SN), the mass of the tertiary, and their SMA. We also present the fraction of systems out of all the runs that remained bound after the SN (column 9), and the fraction of triple systems that remained bound out of all the surviving binaries (column 10). We also show the fraction of systems at which one of the binary members crossed the inner Roche radius ($R_{\rm Roche,\,in}$; see equation 34) out of all binaries. The last column shows the fraction of systems of which one of the binary members crossed their tertiary Roche radius ($R_{\rm Roche,\,out}$; see equation 31) out of all *surviving triple* systems. For NS–NS and BH–BH cases we considered two SN explosions. MC represents Monte Carlo runs (see the text and Table 2 for more details). The details are specified in the text and for completeness we reiterate our Monte Carlo initial conditions here. $\rm MC^{1}$ refers to the Monte Carlo choices for a_1, which is chosen to be uniform in log space between $5\,\rm R_\odot$ and $1000\,\rm R_\odot$. $\rm MC^{2,EC}$, refers to the choice of a_2, from a uniform in log distribution with a minimum a_2 that is consistent with $\varepsilon = 0.1$ and maximum of 10 000 AU. The density of binary systems in this case is consistent with a_2^{-3}, and thus we label it 'EC' for extreme cusp. $\rm MC^{2,BW}$ refers to the Monte Carlo choices of a_2 to be uniform, which is consistent with density of a_2^{-2} with a minimal value 100 AU and a maximum value of 0.1 pc (which is representative of a distribution around an SMBH; e.g. Bahcall & Wolf 1976). Note that the inner and outer SMA also satisfy $\varepsilon = 0.1$ criteria. In all of our Monte Carlo runs, the inner and outer eccentricities were chosen from uniform distribution, the mutual inclination was chosen from an isotropic distribution. The inner and outer arguments of pericentre and the mean anomaly were chosen from uniform distributions. Interestingly, we note that around 10 per cent survived inner binaries in BHB systems obtain hypervelocity. Note that survival rate for binaries and triples refer to the systems that are bound instantaneously post-SNe. The inner binaries that crossed the Roche limit of each other and the binary systems that crossed the Roche limit of the tertiary body are included in the count of survived systems since the systems that are undergoing mass transfer still stay bound post-SNe instantaneously. We provide their percentages in separate columns for clarity. †Note that $1075.5\,\rm R_\odot = 5$ au.

Name	Sim	m_1 $\rm M_\odot$	$m_{1,n}$ $\rm M_\odot$	m_2 $\rm M_\odot$	$m_{2,n}$ $\rm M_\odot$	m_3 $\rm M_\odot$	a_1 $\rm R_\odot$	a_2 AU	Per cent Bin out of total	Per cent Triples out of Bin	Per cent in $R_{\rm Roche,\,in}$ out of Bin	Per cent in $R_{\rm Roche,\,out}$ out of 3	Per cent escaped Bin
NS–LMXB	(a)	4	1.4	1	1	3	$\rm MC^{1}$	$\rm MC^{2,\,EC}$	4	0	0	0	100
	(b)	4	1.4	1	1	4×10^6	$\rm MC^{1}$	$\rm MC^{2,\,EC}$	4	94	0	4	6
	(c)	4	1.4	1	1	4×10^6	$\rm MC^{1}$	$\rm MC^{2,\,BW}$	4	99	0	2	1
	(a5)	4	1.4	1	1	3	1075.5†	$\rm MC^{2,\,EC}$	0.2	19	0	25	0
	(b5)	4	1.4	1	1	4×10^6	1075.5†	$\rm MC^{2,\,EC}$	1	100	0	33	0
	(c5)	4	1.4	1	1	4×10^6	1075.5†	$\rm MC^{2,\,BW}$	0.3	100	0	15	0
BH–LMXB	(d)	9	7	1	1	3	$\rm MC^{1}$	$\rm MC^{2,\,EC}$	11	1	24	13	99
	(e)	9	7	1	1	4×10^6	$\rm MC^{1}$	$\rm MC^{2,\,EC}$	11	99	24	7	1
	(f)	9	7	1	1	4×10^6	$\rm MC^{1}$	$\rm MC^{2,\,BW}$	10	92	25	2	8
	(d5)	9	7	1	1	3	1075.5†	$\rm MC^{2,\,EC}$	1	15	0	13	0.1
	(e5)	9	7	1	1	4×10^6	1075.5†	$\rm MC^{2,\,EC}$	1	100	2	17	0
	(f5)	9	7	1	1	4×10^6	1075.5†	$\rm MC^{2,\,BW}$	1	100	2	14	0
NS–BH	(g)	4	1.4	10	10	3	5	1000	33	0	0	0	100
	(h)	4	1.4	10	10	3	5	$\rm MC^{2,\,EC}$	33	0	0	0	100
	(i)	4	1.4	10	10	4×10^6	5	$\rm MC^{2,\,BW}$	33	99	0	0	1
	(j)	4	1.4	10	10	4×10^6	$\rm MC^{1}$	$\rm MC^{2,\,EC}$	12	71	0	2	29
	(k)	4	1.4	10	10	4×10^6	5	1000	33	100	0	1	0
	(g5)	4	1.4	10	10	3	1075.5†	1000	2	22.4	0	3	0.1
	(h5)	4	1.4	10	10	3	1075.5†	$\rm MC^{2,\,EC}$	2	29	0	11	0.2
	(i5)	4	1.4	10	10	4×10^6	1075.5†	$\rm MC^{2,\,BW}$	2	100	0	7	0
	(j5)	4	1.4	10	10	4×10^6	1075.5†	$\rm MC^{2,\,EC}$	1	100	0	10	0
	(k5)	4	1.4	10	10	4×10^6	1075.5†	1000	2	100	0	74	0
								1st | 2nd	1st | 2nd	1st | 2nd	1st | 2nd	1st | 2nd	1st | 2nd
NS–NS	(l)	5	1.4	4	1.4	3	5	1000	20 | 0	0 | 0	0 | 0	0 | 0	0 | 7
(2 × SN)	(m)	5	1.4	4	1.4	3	5	$\rm MC^{2,\,EC}$	20 | 0	0 | 0	0 | 0	0 | 0	100 | 0
	(n)	5	1.4	4	1.4	4×10^6	5	$\rm MC^{2,\,BW}$	20 | 11	98 | 43	0 | 0	0 | 0	2 | 57
	(o)	5	1.4	4	1.4	4×10^6	5	1000	20 | 10	100 | 93	0 | 0	3 | 0	0 | 7
	(l5)	5	1.4	4	1.4	3	1075.5†	1000	1 | 0	6 | 50	0 | 0	0| 0	0 | 0
	(m5)	5	1.4	4	1.4	3	1075.5†	$\rm MC^{2,\,EC}$	1 | 0	17 | 50	0 | 0	21 | 50	0 | 0
	(n5)	5	1.4	4	1.4	4×10^6	1075.5†	$\rm MC^{2,\,BW}$	1 | 0.3	100 | 100	0 | 0	9 | 35	0 | 0
	(o5)	5	1.4	4	1.4	4×10^6	1075.5†	1000	1 | 0.3	100 | 100	0 | 0	84 | 81	0.1 | 0
BH–BH	(p)	31	30	15	14	3	5	1000	47 | 0	0 | 0	0 | 0	0 | 0	100 | 100
(2 × SN)	(q)	31	30	15	14	3	5	$\rm MC^{2,\,EC}$	47 | 0	1 | 0	0 | 0	0 | 0	99 | 100
	(r)	31	30	15	14	4×10^6	5	$\rm MC^{2,\,BW}$	47 | 29	87 | 83	0 | 0	0 | 0	13 | 17
	(s)	31	30	15	14	4×10^6	5	1000	47 | 32	99 | 98	0 | 0	1 | 0	1 | 2
	(p5)	31	30	15	14	3	1075.5†	1000	4 | 0	9 | 88	0 | 0	3 |14	0.2 | 0
	(q5)	31	30	15	14	3	1075.5†	$\rm MC^{2,\,EC}$	4 | 0.2	14 | 100	0 | 0	9| 19	0.4 | 0
	(r5)	31	30	15	14	4×10^6	1075.5†	$\rm MC^{2,\,BW}$	4 | 2	99 | 100	0 | 0	5 | 4	0 | 0
	(s5)	31	30	15	14	4×10^6	1075.5†	1000	4 | 2	100 | 100	0 | 0	54 | 52	0 | 0

This paper has been typeset from a TEX/LATEX file prepared by the author.